Memoirs of the Faculty of Engineering, Nagoya University
Vol. 38, No. 1 (1986)

STUDY OF WAVEGUIDE-TYPE OPTICAL SEPARATORS USING ACOUSTO-OPTIC EFFECTS

NOBUO GOTO, YASUMITSU MIYAZAKI* and YASUO AKAO**

Department of Electrical Engineering

(Received May 28, 1986)

Abstract

Optical active devices using acousto-optic (A-O) interaction by a surface acoustic wave (SAW) are expected to play an important roll in optical communication and signal processing. In this device using collinear A-O interaction, wavelength-multiplexed optical signals can be controlled by frequency-multiplexed SAWs. The purpose of this study is to develop an A-O separator and to clarify its potential use in signal processing.

First, characteristics of the separator are theoretically discussed. Then the results are experimentally verified with devices consisting of $ZnS/Ta_2O_5/Nb_2O_5$ multilayered films on Y-X $LiNbO_3$ substrates. Next, to improving the A-O interaction efficiency and temperature independency, material combinations of the device are investigated. The design of effective SAW waveguides is also demonstrated for a Ta_2O_5 strip on a $LiNbO_3$ substrate. Finally, channel waveguide devices and their applications to signal processing such as signal exchanging and matrix multiplication are discussed.

CONTENTS

* Department of Information Engineering, Toyohashi University of Technology.
** Emeritus Professor.

1. Introduction

In optical communication and signal processing systems, various types of waveguide devices have been studied.[1~4] Wavelength-division-multiplexing in optical communication is expected to increase the transmission capacity and to enlarge the potential of the signal processing system.[5,6] Tunable wavelength separators and filters, which are indispensable for multi-wavelength communication system, have been demonstrated using acousto-optic (A-O)[7~9] and electro-optic[10~12] effects. The tunable characteristics of these devices can compensate for perturbation effects in multiplex systems due to the wavelength deviation of lasers, or improve its potential for use in various kinds of multi-wavelength systems. Compared to electro-optic devices, A-O waveguide devices have the advantage of being independently controlled for several different-wavelength optical signals by surface acoustic waves (SAWs) of several corresponding different frequencies. Furthermore, the A-O devices can be composed of amorphous films on piezoelectric or even non-

piezoelectric substrates.[13] Monolithic integration with photo detectors is possible when the device is composed on silicon substrates.[14~16]

The purpose of this study is to develop A-O tunable separators, filters and switches for optical signals in a wide wavelength range. These devices have the following features: (i) The guided optical signals are separated into two waveguides with the same polarization; (ii) high A-O interaction efficiency with narrow filtering pass bandwidth is realized because of the collinear interaction; (iii) several optical signals with different wavelengths are independently controlled by frequency multiplexed SAWs; and (iv) the device has several controllable parameters such as refractive indices and film thicknesses. By using these excellent features, this A-O device can be applied to a variety of signal processors.

This paper, beginning with the introduction, consists of ten chapters The principle of wavelength separation is described in Chapter 2. Theoretical characteristics of switching and tunable wavelength separation are discussed for a device consisting of $ZnS/Ta_2O_5/Nb_2O_5$ thin layered films on a Y-cut X-propagation (Y-X) $LiNbO_3$ substrate in Chapter 3. The theoretical results of switching and wavelength separation are experimentally verified in Chapters 4 and 5, respectively. Temperature dependence is discussed to realize temperature independent devices in Chapter 6. In Chapter 7, the strain distribution of the SAW in layered media is calculated to improve the A-O interaction efficiency. Further, SAW channel waveguides are investigated to decrease the required SAW power for switching in Chapter 8. More practical devices consisting of channel waveguides and their applications to signal processing are discussed in Chapter 9. Finally, this paper is summarized in Chapter 10.

2. Basic Description of Separator

2. 1. Introduction

The separator is composed of an optical directional coupler and separating branches. Since the SAW interacts collinearly with optical waves along the coupling region[17], effective A-O interaction is realized compared to non-collinear A-O devices.[2,9] The coupler consists of two parallel waveguides. When the individual waveguides support modes with almost equal propagation constant, the coupler degenerates (degenerate device); whereas, the coupler does not degenerate (nondegenerate advice) when the modes have different propagation constants. Switching mechanisms in these two kinds of devices are clarified in this chapter.[18,21]

2. 2. Principle of Wavelength Separation

A basic structure of the separator is illustrated in Fig. 2. 1. In the coupling region with a thin middle layer, the optical waves in the two waveguides couple strongly. The optical waves are considered to be composed of fundamental even and

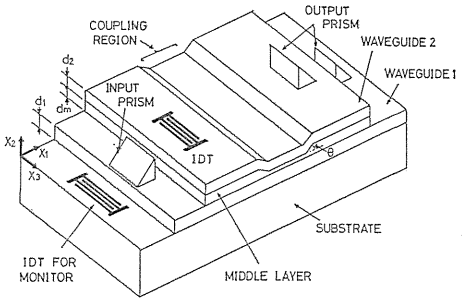

Fig. 2. 1. Basic structure of multilayered separator.

odd modes in one waveguide system.[22] This device uses A-O mode conversions between the optical even and odd modes by the SAW. The main difference of switching mechanisms between the degenerate and nondegenerate devices exists in the optical wave separation in the separating branches.[23] In a branch of small propagation-constant difference Δk between the two waveguides for the infinite middle layer thickness ($d_m=\infty$) and a fairly large branching angle θ, the branch acts as a power divider due to mode conversions. On the other hand, a branch of large Δk and small θ acts as a mode splitter, where mode conversions are negligible. The condition for the mode splitter is given by[24,25]

$$\Pi=\Delta k/(\theta\sqrt{k_{av}{}^2-n_m{}^2k_0{}^2})\gtrsim 0.43, \tag{2·1}$$

where k_{av} is an average propagation constant of the two waveguides for $d_m=\infty$. Using the propagation constants of the two individual waveguides, k_1 and k_2, k_{av} is given by $(k_1+k_2)/2$. The symbol n_m is a refractive index of the middle layer and k_0 is a propagation constant in free space.

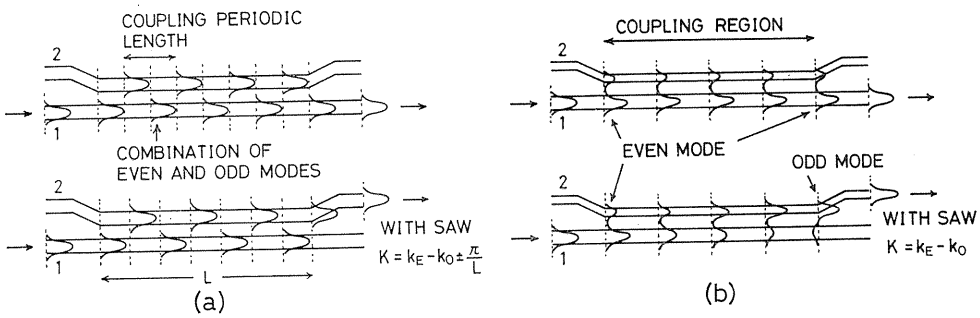

Fig. 2. 2. Schematic descriptions of the switching mechanism in (a) degenerate and (b) nondegenerate devices.

Schematic switching mechanisms are shown in Fig. 2. 2. In the degenerate coupler, the optical wave coupled into waveguide 1 has optical fields of the combination of the even and odd modes. Since the propagation constants of these modes are different, the superposition of these modes shows a periodically transferred propagation between the two waveguides. When the length of the coupling region L is chosen to be integer multiples of the coupling periodic length Λ, the optical power is coupled out from the waveguide 1, because the branch acts as a power divider. When the SAW interacts with the optical waves under nearly Bragg conditions as

$$K=k_E-k_O\pm\pi/L, \tag{2·2}$$

the optical periodic length Λ is perturbed and the accumulation of the effect along the interaction length L makes the optical power concentrate in waveguide 2, where K is the propagation constant of the SAW; k_E and k_O are those of the optical even and odd modes. The plus-minus signs in Eq. (2·2) correspond to the lengthened and shortened shift of Λ due to A-O interaction, respectively.

The switching mechanism in the nondegenerate device is shown in Fig. 2. 2(b).

The optical wave coupled in waveguide 1 propagates in the even mode and separates out from the same waveguide 1, provided that the propagtion constant of waveguide 1 is larger than that of waveguide 2. When the SAW interacts under the Bragg condition as

$$K=k_E-k_O, \tag{2·3}$$

the optical power in the even mode is converted to that in the odd mode along the interaction region. Since the separating branch acts as a mode splitter, the converted optical power in the odd mode transfers to waveguide 2.

The switching characteristics are theoretically clarified by solving mode coupling equations between the even and odd modes with the SAW along the interaction region.[17,20,26,27] In the degenerate device, the switched optical power $P_2/(P_1+P_2)$ depends on the acoustic power as shown in Fig. 2. 3(a), where g is the mode conversion coefficient and is proportional to square root of the SAW power; ΔK is the shift from the Bragg condition given by $\Delta K=K-(k_E-k_O)$. The switched optical power is accompanied with a ripple at the SAW angular frequency Ω, except for complete switching at $Lg=\sqrt{3}\pi/2$. The switched optical power depends on $L\Delta K$ as shown in Fig. 2. 3(b). Complete switching is performed at $L\Delta K=\pm\pi$. The interaction length L must be adjusted to be an integer multiple of $\Lambda/2$. These curves are also regarded as the dependence on the SAW frequency.

On the other hand, the similar characteristics in the nondegenerate device are shown in Fig. 2. 4. The switched signal has no ripple at any values of both Lg and $L\Delta K$. Optical waves are completely switched for any interaction length. The asymmetry of optical fields in the two waveguides does not reduce the switching extinction ratio. In the degenerate device the field's asymmetry reduces the ex-

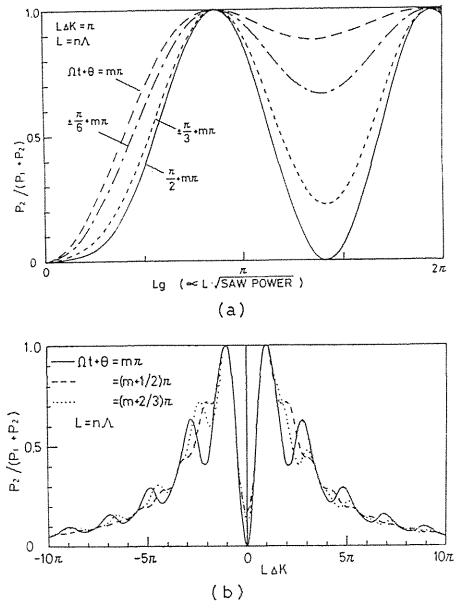

Fig. 2. 3. Dependence of switched optical power on (a) Lg and (b) $L\Delta K$ in the degenerate device.

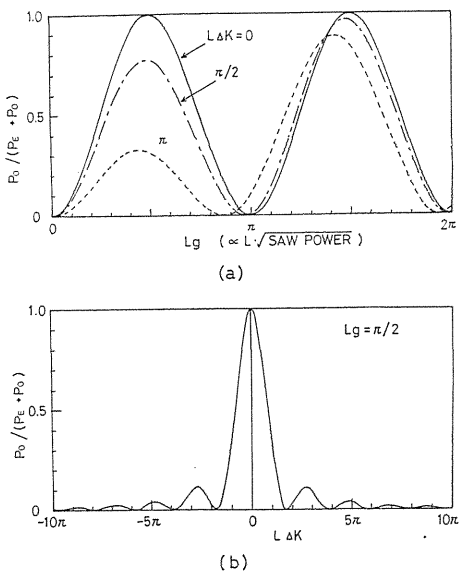

Fig. 2. 4. Dependence of switched optical power on (a) Lg and (b) $L\Delta K$ in the nondegenerate device.

tinction ratio, because the branch acts as a power divider. Furthermore, the dependence on $L\Delta K$ as in Fig. 2. 4(b) indicates that the nondegenerate device has excellent properties as a switch, wavelength separator or filter. Although both types of the device can switch optical power at 100 percent, the nondegenerate one is more convenient for practical use.

3. Theoretical Characteristics for Separator

3. 1. Introduction

Based on the switching characteristics, tunable wavelength separating and filtering properties are theoretically discussed.[28~30] We consider a device consisting of $ZnS/Ta_2O_5/Nb_2O_5$ thin films on a Y-X $LiNbO_3$ substrate, whose materials are used in the experiment described in the next chapter.

3. 2. Optical Coupling between Two Waveguides

Good amorphous films of ZnS, Ta_2O_5 and Nb_2O_5 are easily fabricated by R. F. sputtering.[29,31] The A-O effect must be concentrated in one of the two waveguides to increase the overlap integral of optical and acoustic fields. Since the material of ZnS has a small photoelastic constant, the A-O effect is considered to be larger in the Nb_2O_5 waveguide than that in the ZnS one. The materials of Ta_2O_5 and Nb_2O_5 films have been investigated for use in low-loss optical waveguides possessing high refractive index.[32~34] The dispersion of the refractive index of the constituent materials is measured as shown in Fig. 3. 1, where the data for ZnS and $LiNbO_3$ are quoted from previous works.[35,36] This dispersion of ZnS agrees well with the measured value for ZnS films sputtered in an Ar gas atmosphere with a ZnS target. The films of Ta_2O_5 and Nb_2O_5 were sputtered using Ta and Nb targets in the Ar and O_2 mixed gas atmosphere of the rate $Ar/O_2=4$, respectively. The fabricated films were found to be amorphous using X-ray diffractometry. The refractive index of Nb_2O_5 has stronger dispersion than that of Ta_2O_5 in the short wavelength region. The refractive indices of ZnS, Ta_2O_5, Nb_2O_5 and $LiNbO_3$ at the wavelength $\lambda_0=0.6328\mu$m are 2. 35, 2. 09, 2. 27 and 2. 20 (n_e), respectively. A degenerate coupler is designed by making the propagation constants in the two waveguides equal for $d_m=\infty$. For an example, we consider a coupler of the thicknesses $d_1=0.911\mu$m and $d_2=0.329\mu$m for waveguides 1 and 2, respectively. The propagation constants of the even and odd modes, k_E and k_O, depend on the middle layer thickness as shown in Fig. 3. 2.[37] The periodic coupling length Λ is calculated from the discrepancy between k_E and k_O. Optical fields for the two modes are distributed as shown in Fig. 3. 3. The asymmetry of the fields comes from the asymmetric distribution of the refractive index.

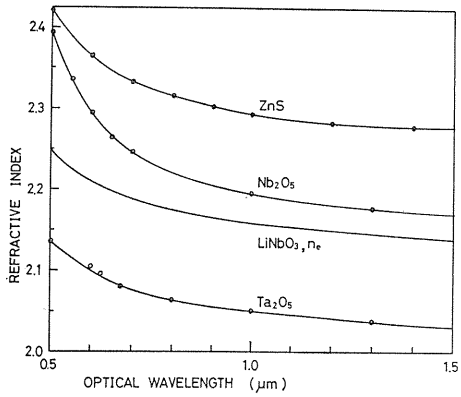

Fig. 3. 1. Dispersions of refractive index.

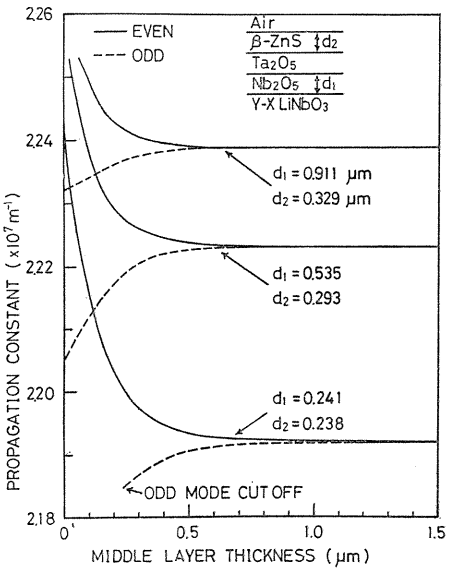

Fig. 3. 2. Mode dispersions of optical even and odd modes.

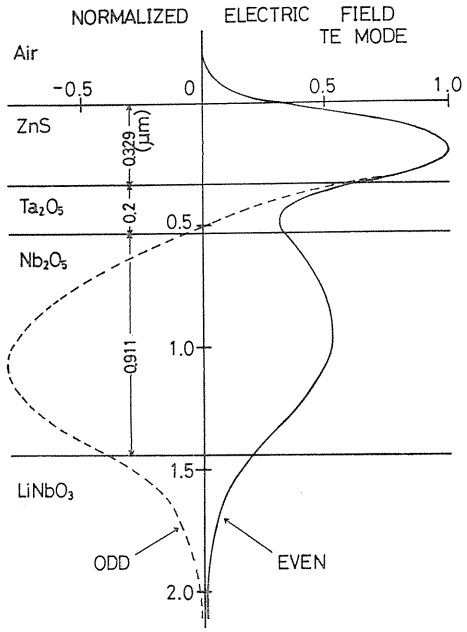

Fig. 3. 3. Distributions of optical electric fields

3. 3. *Wavelength Separating Characteristics*

One of the important characteristics is the use of acoustic power required for complete switching. The power P_a is given by[17]

$$P_a = 2W\Lambda_a\lambda^2(gL)^2/(\pi^3ML^2\gamma_{EO}{}^2) \qquad (3\cdot1)$$

where γ_{EO} is an overlap integral for optical waves and acoustic strains; W and Λ_a are the beam width and the wavelength of the SAW, respectively; M is a physical constant depending on the constituent material.

The overlap integral γ_{EO} includes the photoelastic constants p_{ij}. In the configuration shown in Fig. 1. 1, the components p_{12} of the films and p_{31} of the substrate take part in the A-O interaction. Since the photoelastic constants of Ta_2O_5 and Nb_2O_5 have not been exactly studied, we assume the values as 0. 1, 0. 2 and 0. 3, as tabulated in Fig. 3. 4. Many high

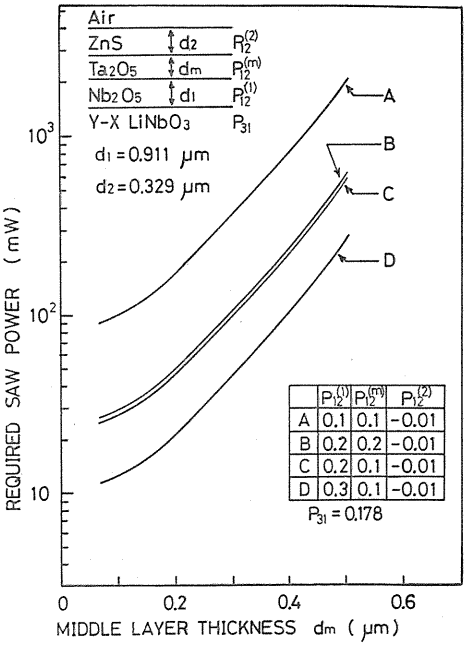

Fig. 3. 4. Required SAW power for complete switching.

refractive index materials have their photoelastic constants around these values. Figure 3. 4 shows the SAW power required for switching with $W=1$ mm and $L=8$ mm at $\lambda_0=0.6328$ μm. Here, the acoustic strains are assumed to be uniformly distributed in the interaction region. It is found that a large difference in p_{12} between waveguides 1 and 2 is necessary to improve the control efficiency.

In wavelength separation, the half-power pass bandwidth $2\Delta\lambda_h$ for filtering is given by

$$2\Delta\lambda_h=2\Delta K_h L/\{|\partial(k_E-k_0)/\partial\lambda|L\}, \tag{3·2}$$

where $2\Delta K_h$ is the bandwidth of the wave number deviation from the Bragg condition. The value $2\Delta K_h$ is derived to be 1.65π from Fig. 2. 4(b). This pass bandwidth is converted to the bandwidth of the SAW frequency f. The frequency is given by

$$f=v|k_E-k_0|/(2\pi), \tag{3·3}$$

where v is the SAW velocity. The velocity of a Rayleigh wave without films on Y-X $LiNbO_3$, that is $v=3.77$ km/s, is used in the calculations. The bandwidth of the SAW frequency $2\Delta f_h$ is derived as

$$2\Delta f_h=(2\Delta K_h L)v/(2\pi L). \tag{3·4}$$

When L is taken to be 8 mm, the $2\Delta f_h$ is calculated as 0.39MHz. In order to characterize the tuning properties, we introduce a tuning sensitivity T_s defined by[7]

$$T_s=|(\delta\lambda/\lambda)/\delta f|, \tag{3·5}$$

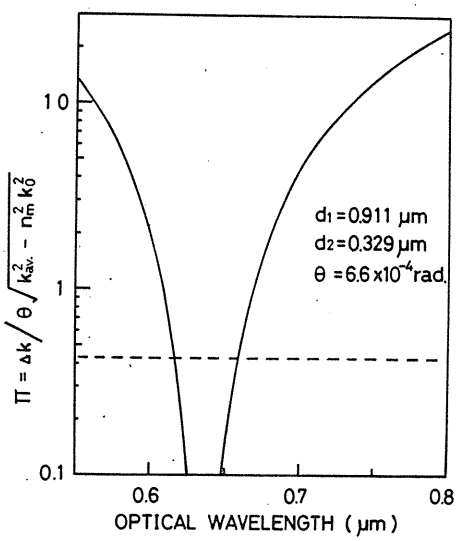

Fig. 3. 5. Wavelength dependence of Π.

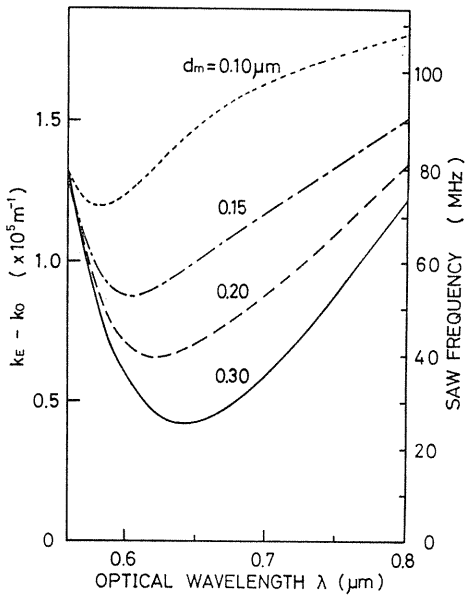

Fig. 3. 6. Wavelength dependence of k_E-k_0. Right-hand scale indicates required SAW frequency.

where $\delta\lambda$ is a shift in the selected optical wavelength due to a change in the acoustic frequency δf.

These characteristics in a device designed to degenerate at $\lambda_0=0.6328\,\mu$m are calculated. The paramater Π as noted in Eq. (2·1) is shown as a function of the optical wavelength in Fig. 3. 5. The branch acts as a power divider in the range of $0.62\mu\text{m}\lesssim\lambda\lesssim0.66\mu\text{m}$. In this wavelength range the device is regarded as degenerate one. At the other wavelength, the optical waves are switched by a mechanism in the nondegenerate device. The dispersion factor $\partial(k_E-k_O)/\partial\lambda$ is obtained by solving the characteristic equation for optical guided waves. Figure 3. 6 shows k_E-k_O versus λ, considering the material dispersions of the refractive index shown in Fig. 3. 1. Tuning of the SAW frequency is also calculated by Eq. (3·3) as shown in the right-hand scale of Fig. 3. 6. The bandwidth $2\Delta\lambda_h$ is shown in Fig. 3. 7. The bandwidth increases rapidly near the designed wavelength λ_0 because the gradient in the curves of k_E-k_O becomes small. Except for the region near λ_0, an increase in the middle layer thickness makes the bandwidth narrow. The wavelength of divergent points shifts to the short-wavelength-side, especially in the case of a thin middle layer, because of the material dispersion of the refractive index. The tuning sensitivity T_s depends on λ as shown in Fig. 3. 8. The wavelength deviation of the order of some tens Å is controlled by a SAW frequency change of 1MHz. Figure 3. 9 shows the dependence of the required SAW power on λ, where p_{12} is assumed to be 0. 1 and 0. 3 for the middle layer and waveguide 1, respectively.

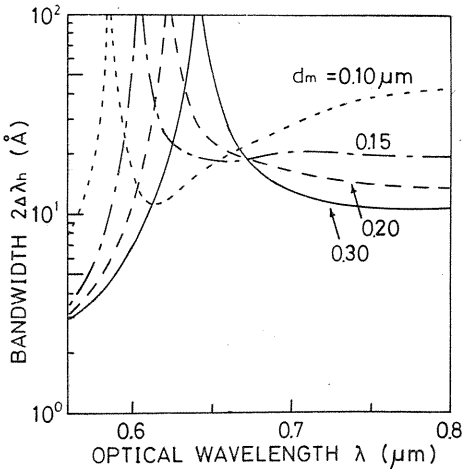

Fig. 3. 7. Half-power pass bandwidth.

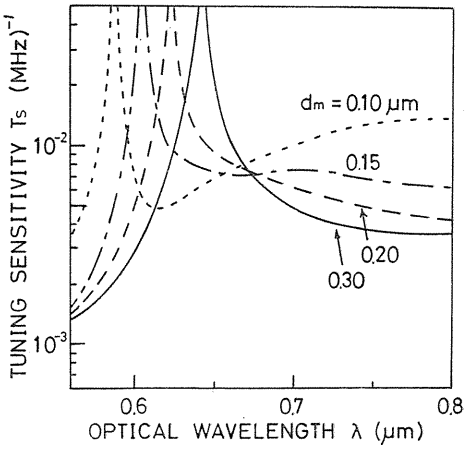

Fig. 3. 8. Tuning sensitivity.

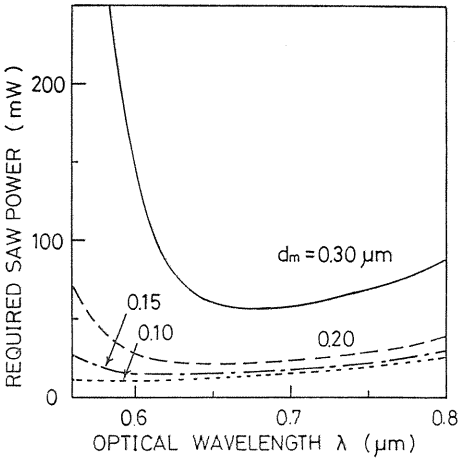

Fig. 3. 9. Required SAW power for switching.

The coupling periodic length becomes short as the wavelength diverges from λ_0. In spite of this shorter coupling length, which makes the SAW power small, the decrease of γ_{EO} makes the power large at wavelengths away from λ_0. The switching power is comparable to other A-O devices. The characteristics for filters and separators can be improved by using better material combinations and film thicknesses.

4. Switching and Separation Properties

4. 1. Introduction

Optical switching properties are important as basic function for separators and filters. In this chapter, optical switching is experimentally investigated in both degenerate and nondegenerate devices consisting of $ZnS/Ta_2O_5/Nb_2O_5$ films on Y-X $LiNbO_3$.[19~21] The results prove the theoretical properties described in the previous chapters. The switching mechanism is also verified.

4. 2. In Degenerate Device

The two waveguides of a degenerate device are carefully fabricated to have the same propagation constants for infinite middle layer thickness as $d_1=0.638\,\mu$m and $d_2=0.305\,\mu$m. The middle layer thickness d_m was $0.203\,\mu$m in the coupling region and $1.0\,\mu$m in the non-coupling parts. The separating branch angle θ was 7×10^{-4} rad.. Surface acoustic waves are excited by an Al interdigital transducer (IDT) of the thickness of $0.3\,\mu$m which was fabricated on waveguide 2.

The experimental setup is shown in Fig. 4. 1. A laser beam of 0.6328μm was coupled into waveguide 1 with a rutile prism coupler in TE_0 mode. The separated beams were detected with photomultipliers. Figure 4. 2 shows a photograph of the guided optical wave in the coupling region. The coupling periodic length Λ is found to be $132\,\mu$m. The dark lines in the right side show the IDT which consists of 10 finger pairs, the aperture width of 3.5 mm and the periodic length of $132\,\mu$m. The optical propagation loss is about 1.5 dB/cm. The interaction length L is 8 mm.

A photograph of the optical switching due to the applied SAW power is shown in Fig. 4. 3. The applied electric power in the IDT was 6.3 W at 28.6 MHz. The light outputs were transferred with the R. F. electric power as shown in Fig. 4. 4. The electric power of 6.3 W was converted to the acoustic power of about 0.75 W.

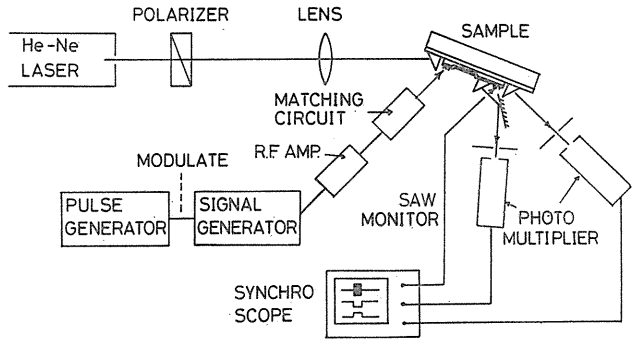

Fig. 4. 1. Experimental setup.

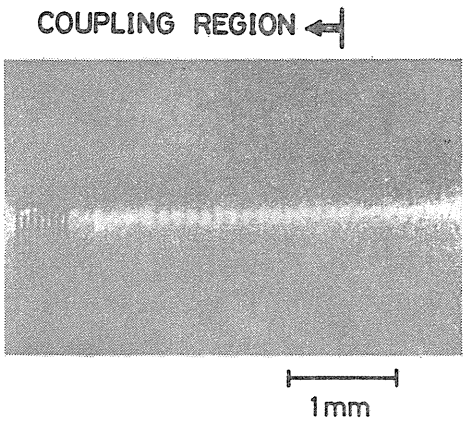

Fig. 4. 2. Scattered light in the propagating optical beam.

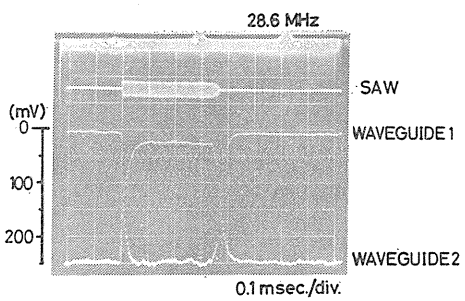

Fig. 4. 3. Optical outputs switched by SAW pulse.

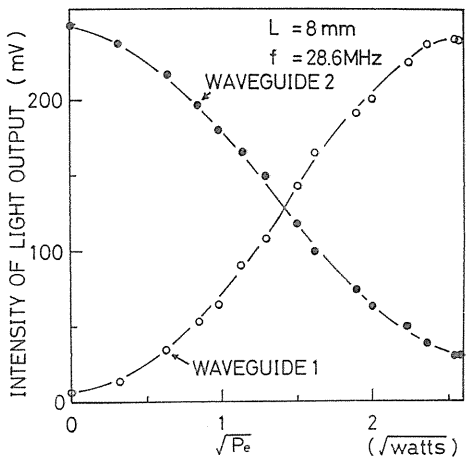

Fig. 4. 4. Exchanging optical power with R. F. electric power.

The extinction ratio of the switching was about 16 dB and 10 dB for waveguides 1 and 2, respectively. In this device, optical power is concentrated in waveguide 2 at the separating point after the interaction region without the SAW, which means that the coupling length L was adjusted to be $(n+1/2)\Lambda$ (n is an integer). Figure 4. 5 shows the frequency dependence of the output intensity from waveguide 2 with the theoretical result. The reduction of the peak at 29. 1 MHz is mainly caused by the decrease of the SAW power.

In the next step, the coupling prism was attached on waveguide 2 in the coupling region in order to investigate the dependence of A-O interaction on the interac-

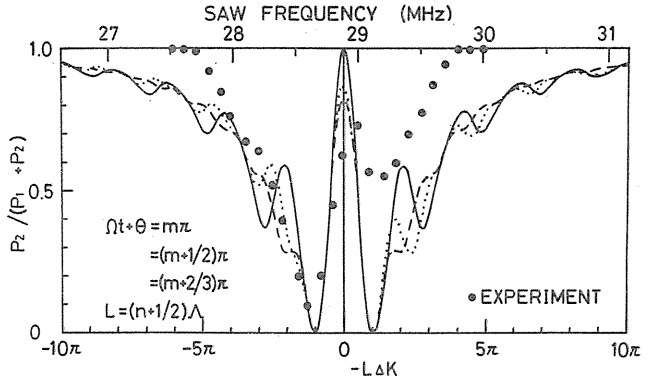

Fig. 4. 5. Frequency dependence of the output at $L \simeq 8$ mm.

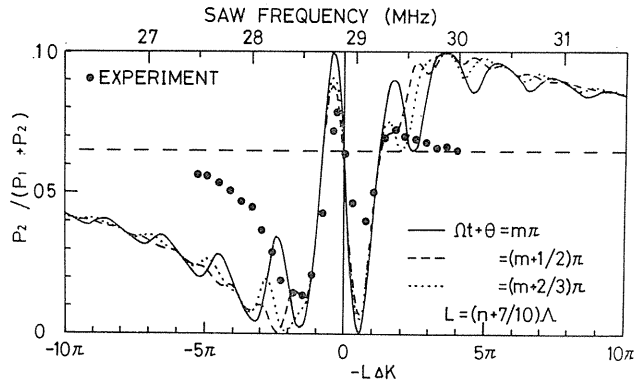

Fig. 4. 6. Frequency dependence of the output at $L\simeq 7$ mm.

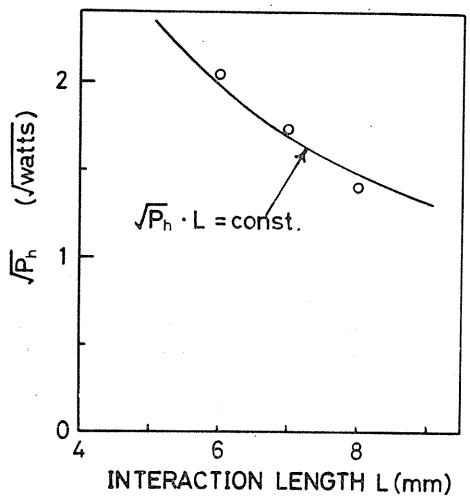

Fig. 4. 7. Required R. F. power for 50 percent switching.

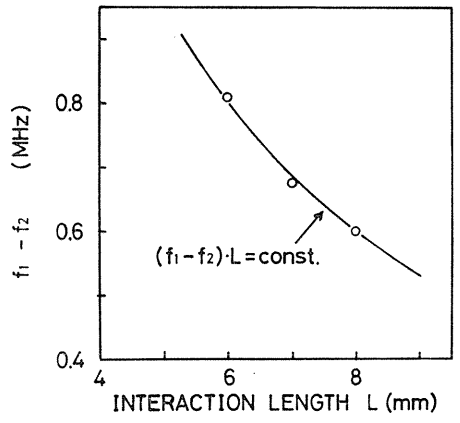

Fig. 4. 8. The difference of the two peaks in the frequency dependence.

tion length. The frequency dependence for $L\simeq 7$ mm is shown in Fig. 4. 6. The interaction length is not an integer multiple of Λ. The theoretical curves are for $L=(n+7/10)\Lambda$. These experimental data agree well with the theoretical results. Figure 4. 7 shows the required SAW power with the interaction length L, where P_h is the R. F. electric power required for 50 percent switching. The results are in good agreement with the theoretical curve of $\sqrt{P_h}L=$constant. The frequencies of the two peaks in the frequency dependence, that is $f_1=28.6$ MHz and $f_2=29.1$ MHz in Fig. 4. 5, are measured with L as shown in Fig. 4. 8. The theoretical value f_1-f_2 is inversely proportional to L.

In order to confirm the theoretical meaning of the two peaks at f_1 and f_2, the change of the optical output was measured by shifting the interaction length. The output from the prism fixed on waveguide 1 changed with the interaction length as shown in Fig. 4. 9. Since the SAW power was about 40 mW, only several percent of optical power is switched. The output shown in Fig. 4. 9(a) indicates the

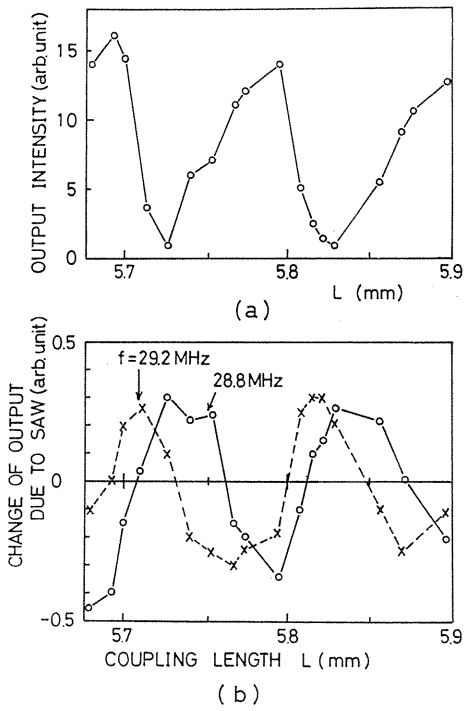

Fig. 4. 9. (a) Output intensity without the SAW and (b) change of the output intensity due to A-O interaction.

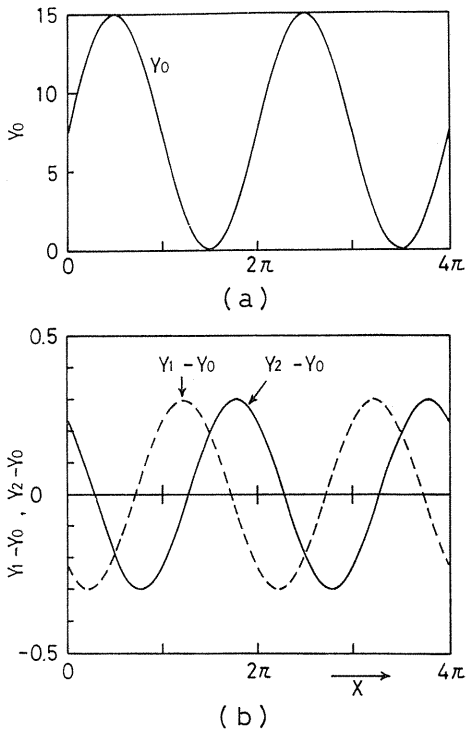

Fig. 4. 10. Sinusoidal curves corresponding to the output optical power in Fig. 4. 9, where the curves are given as
$Y_0=7.5(1+\sin X)$
$Y_1=7.5\{1+0.975\sin(X-0.01\pi)\}$
$Y_2=7.5\{1+0.975\sin(X+0.01\pi)\}$.

appearance of the coupling light beam between the two waveguides. The change of light output due to the SAW is shown in Fig. 4. 9(b). The two curves for the two frequencies show the sinusoidal curves, where the curves are different in the phase by a quarter of the periodic length. These results are compared to the sinusoidal curves as shown in Fig. 4. 10. The basic curve Y_0 is a sinusoidal curve of the amplitude 7. 5, which was selected to fit the scale of the measured intensity. The two curves Y_1 and Y_2 correspond to the optical output with the SAW of the two different frequencies. The phase shifts of Y_1 and Y_2 from Y_0 are -0.01π and $+0.01\pi$, respectively. Figure 4. 10(b) corresponds to the experimental results in Fig. 4. 9(b). It is found from comparison with theoretical results that the coupling of the optical beam around $L=5\sim6$ mm is considered to shift to the left side in Fig. 4. 9(a) by the SAW of 28. 8MHz, which means that the periodic coupling length becomes short and the accumulation of the deviation of Λ causes the shift of the optical coupling beam to the left side. While, the SAW of 29. 2 MHz made the optical beam shift to the right side.

4. 3. In Nondegenerate Device

A device was fabricated with the same materials as those in the degenerate device. The film thicknesses are $d_1=0.590\,\mu$m and $d_2=0.285\,\mu$m. The middle layer thickness d_m is $0.180\,\mu$m and $0.7\,\mu$m in the coupling and non-coupling region, respectively. The waveguides become degenerate at $d_2=0.300\,\mu$m. The propagation constants of waveguides 1 and 2 were measured as $k_1=2.227\times10^7\text{m}^{-1}$ and $k_2=2.2195\times10^7\text{m}^{-1}$ at the non-coupling region, respectively. Since k_1 is larger than k_2, the optical wave in the even mode becomes the fundamental mode in waveguide 1 through the separating branch. The phase-mismatch of the waveguides reduced the optical periodic coupling power to about 50 percent in this device. The separating branch angle θ was 6.6×10^{-4}rad.. At $\lambda_0=0.6328\,\mu$m, the parameter II in Eq. (2·1) is calculated to be 14. Therefore, the branch acts as a complete mode splitter. Surface acoustic waves were excited by an IDT consisting of 10 finger pairs with the aperture width of 3.5 mm. The periodic length is $50\,\mu$m, which was determined by Eq. (2·3).

Figure 4. 11 shows the switching with the applied electric power at 71.2 MHz. The converted SAW power of about 0.5 W switched 90 percent of the optical power. By comparison with the theoretical curves in Fig. 2. 4, the SAW power of 0.6 W is required in order to complete switching. The extinction ratio for waveguide 2 is more than 20dB. The higher extinction ratio is more easily realized in a nondegenerate device than in a degenerate one. The frequency dependence is shown with the theoretical curve in Fig. 4. 12. The rapid change with frequency is due to the SAW reflection at another IDT with which the SAW is monitored. The half-power bandwidth is regarded as about 0.4 MHz, which is in fairly good agreement with a theoretical value of 0.39 MHz.

In the following experiments the input prism coupler was placed on waveguide 2 in the coupling region. The incident optical mode in the waveguide is selected by setting the incident angle θ_i into the input prism. The A-O interaction length

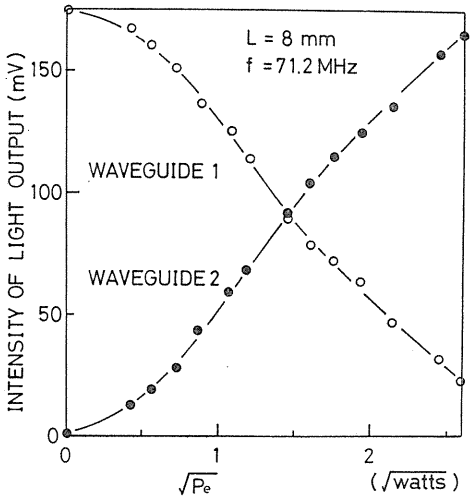

Fig. 4. 11. Exchanging optical power with R. F. power.

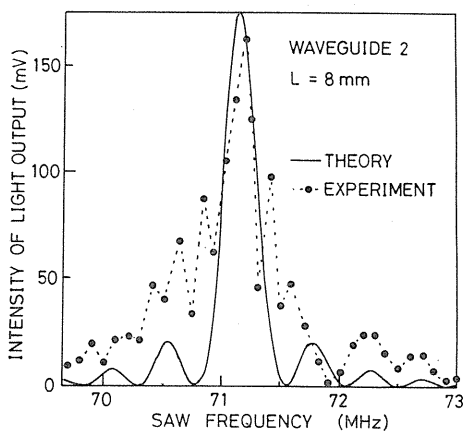

Fig. 4. 12. Frequency dependence of the output.

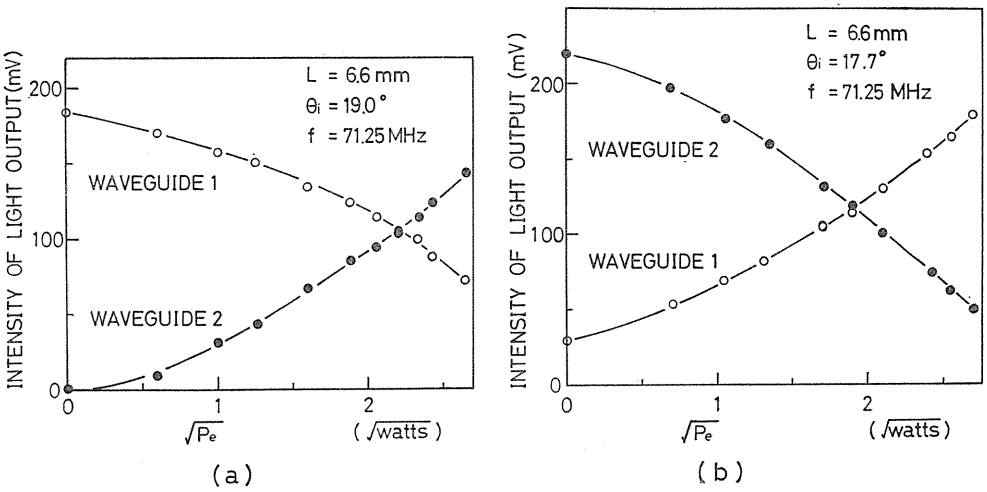

Fig. 4. 13. Exchanging optical power at (a) $\theta_i=19.0°$ and (b) 17.7°.

L was 6.6 mm. Figure 4. 13 shows the optical outputs from the two waveguides versus the applied electric power. The incident guided waves were excited in the even and odd modes in Fig. 4. 13 (a) and (b), respectively. The outputs from waveguides 1 and 2 are regarded as the power in the even and odd modes at the separating branch. The increased output with increasing SAW power is the converted power into the other mode due to A-O interaction. The theoretical switching mechanisms discussed in Chapter 2 are verified by these experiments.

5. Wavelength Selecting Properties

5. 1. Introduction

One of the excellent features in A-O switches exists in the simultaneous control for several optical signals with different wavelengths, compared to electro-optic devices.[12,37] In this section, the experimental results on the wavelength separation and tunable filtering are described and compared with theoretical results discussed in Chapter 3.[38,39] The findings prove that this type of device has potential for wavelength separators and tunable filters in the wavelength-division-multiplexing communications and signal processing systems.

5. 2. Experiments

A device was fabricated to be almost degenerate at $\lambda_0=6328$ Å. The thicknesses are $d_1=0.95\,\mu$m and $d_2=0.33\,\mu$m. The middle layer thickness d_m is $0.30\,\mu$m and $0.70\,\mu$m in the coupling and non-coupling regions, respectively. The branch angle θ is about 7×10^{-4} rad.. The interaction length is 4mm. The experimental setup is illustrated in Fig. 5. 1. The wavelengths of the incident beams were $\lambda_0=6328$ Å (He-Ne laser) and $\lambda_1=7791$ Å (laser diode LD). The discrepancy of the propagation constant between the optical even and odd modes, k_E-k_O, was measured to be $3.7\times10^4\mathrm{m}^{-1}$ and $1.2\times10^5\mathrm{m}^{-1}$ at λ_0 and λ_1, respectively. Surface acoustic waves were

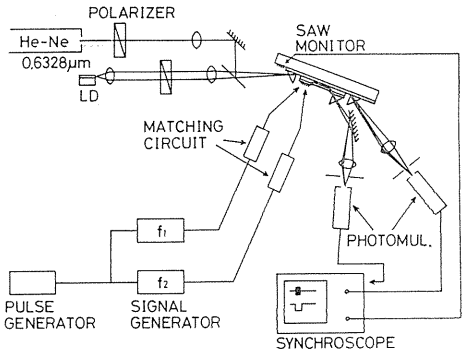

Fig. 5. 1. Experimental setup.

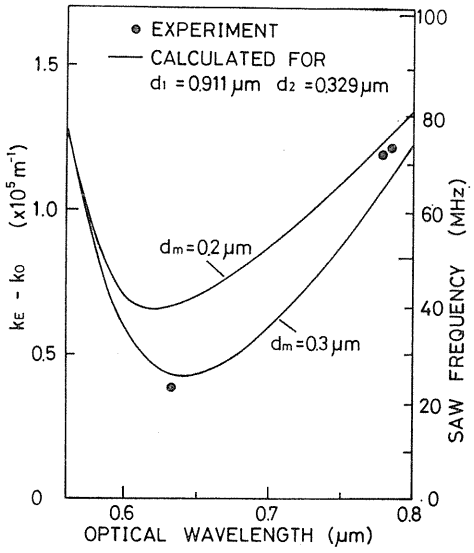

Fig. 5. 2. Wavelength dependence of required SAW frequency.

excited by two IDTs with different periodic lengths. The IDT for lower frequency excitation has 10 pairs with a periodic length of 173 μm and an aperture width of 4.5 mm, and the other IDT for higher frequency excitation has 4 pairs with a periodic length of 52.5 μm and an aperture width of 3.0 mm. The SAW frequency required for switching was shown in Fig. 5. 2. For both the wavelength λ_0 and λ_1, the switching mechanism is regarded as that of the nondegenerate switch.

When the laser beams of λ_0 and λ_1

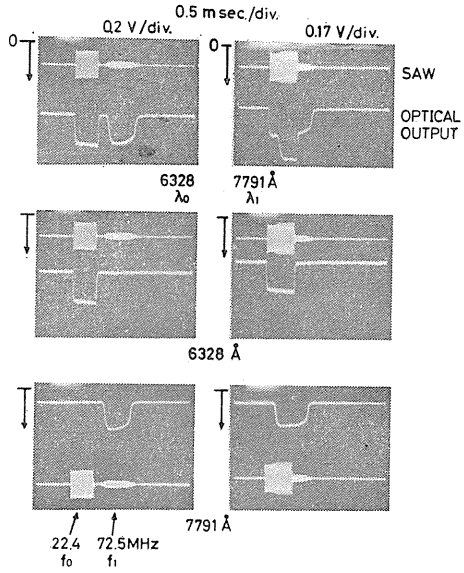

Fig. 5. 3. Wavelength-selective control for two optical wavelengths.

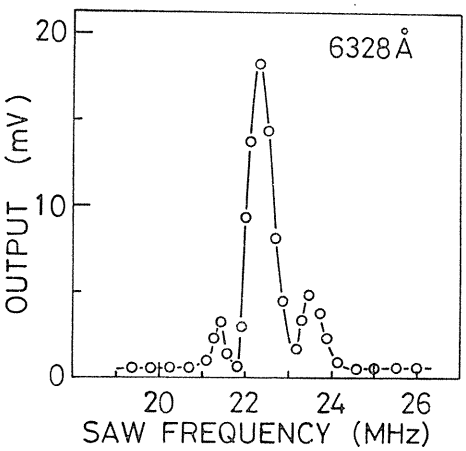

Fig. 5. 4. Frequency dependence of switched optical output for λ_0=6328 Å.

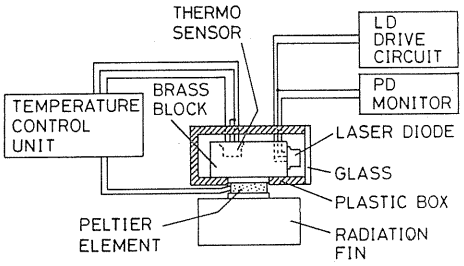

Fig. 5. 5. Temperature control equipment for LD.

were coupled into waveguide 1 in the TE mode, the optical output from waveguide 2 increased with SAW pulses as shown in Fig. 5. 3. The photographs on the right show optical switching due to overlapping SAW pulses of two frequencies, $f_0=22.4$ MHz and $f_1=72.5$ MHz. Almost 20 percent of the optical guided power with λ_0 and λ_1 was separated by the SAW power of 60mW of f_0 and f_1, respectively. The guided optical waves of two different wavelengths were independently controlled by the SAWs with two frequencies. Wavelength-multiplexed optical signals can be controlled by frequency-multiplexed SAWs with one A-O element. This is one of the most attractive features in collinear A-O devices. The switched optical output at λ_0 depended on the SAW frequency as shown in Fig. 5. 4. The half power bandwidth is 0.7 MHz, which is in good agreement with the theoretical value of 0.78 MHz for $L=6$ mm.

The wavelength of the LD was changed by a thermal control[40] in order to measure the tunable separating characteristics around the wavelength of 7800Å. The temperature of LD was controlled with a peltier element as show in Fig. 5. 5. The temperature was monitored with a thermo sensor. The temperature stability was in the range of ± 0.01℃. The LD was operated in a single mode in the temperature range of 15~40℃ as shown in Fig. 5. 6. The optical output power is 3 mW. The wavelength of the light emitted from the LD shifted by 2Å/℃ as shown in Fig. 5. 7. The required SAW frequency for the wavelength separation increased with the wavelength as shown in Fig. 5. 8. The tuning sensitivity T_s defined by Eq. (3·5) was evaluated to be about 3.4×10^{-3} MHz^{-1}. The frequency dependence of the separated output beam at 7791Å and 7841Å is shown in Fig. 5. 9. The half-power bandwidth was 1.0 MHz, which is a little wider than the theoretical value of 0.78

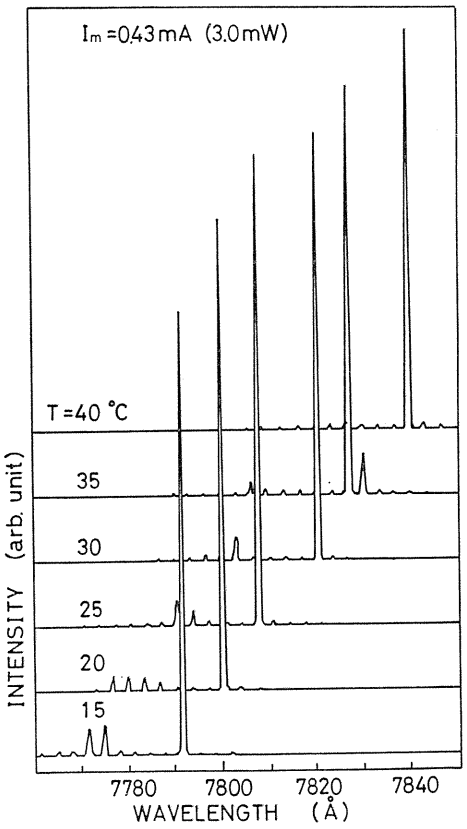

Fig. 5. 6. Spectrum of emitted light from LD.

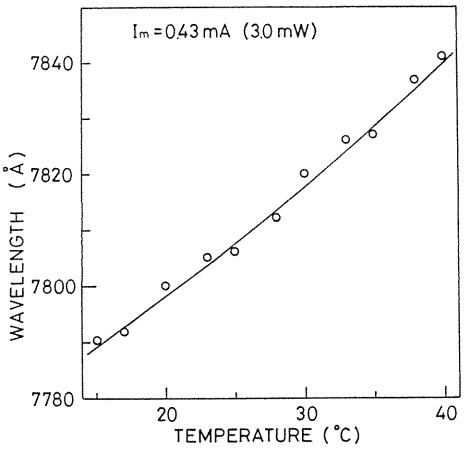

Fig. 5. 7. Wavelength shift due to temperature change.

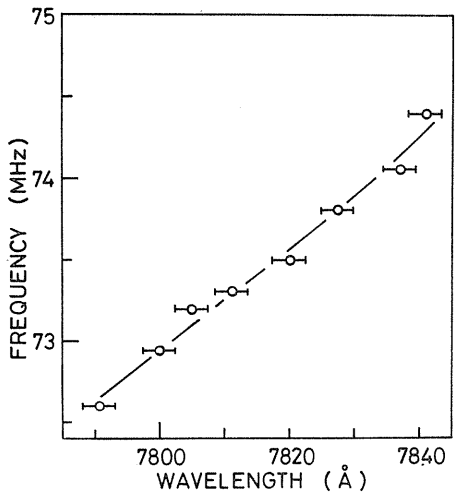

Fig. 5. 8. Wavelength dependence of the SAW frequency.

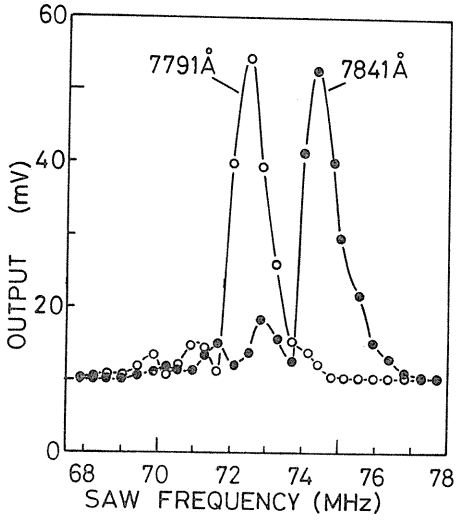

Fig. 5. 9. Frequency dependence for separated two wavelengths.

MHz. This difference was caused by the optical beam spread in the waveguides. The measured bandwidth $2\Delta f_h = 1.0$ MHz is converted to the bandwidth $2\Delta\lambda_h = 27$Å by using the obtained tuning sensitivity T_s. This value is in agreement with the calculated value of 22 Å for the device of $L = 4$mm.

6. Temperature Dependence

6. 1. Introduction

Temperature dependence of waveguide devices is one of the important characteristics for practical use. Recently, thermo-optic deflectors and switches have been demonstrated, utilizing actively the refractive-index deviation at the surface induced by a thermal increase.[41] On the contrary, the temperature independence of optical waveguides was investigated in only a few material combinations.[42] In this chapter, the temperature dependence is investigated to realize temperature independent A-O devices.[39,43]

6. 2. Experiment in a Nondegenerate Device

First, the temperature dependence in the nondegenerate device described in Section 4. 3 is measured. The experimental setup is schematically shown in Fig. 6. 1. The device was set in a thermo-box with a room space of $120 \times 120 \times 100$mm^3. The temperature was changed slowly with the rate of about 5℃/hour, using peltier elements. The laser beam of 6328 Å was coupled into waveguide 1 using a rutile prism.

The SAW frequency f, tuned so that the maximum conversion from waveguide 1 to waveguide 2 was obtained was measured as a function of temperature T in Fig. 6. 2. The gradient of the resultant temperature dependence of the frequency

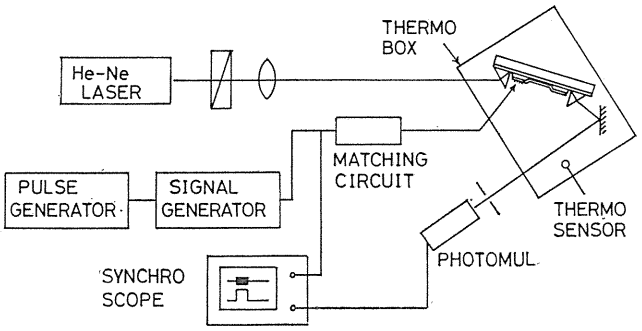

Fig. 6. 1. Experimental setup.

is approximately -0.20MHz/℃. This value is fairly large for the practical use, because the half-power bandwidth is about 0.4 MHz. In order to reduce the temperature dependence, a theoretical discussion is presented in the next section.

6. 3. Theoretical Discussion

The tuning frequency deviation due to the SAW velocity fluctuation is at most 0.007MHz/℃. On the contrary, the frequency deviation due to the fluctuation in propagation constant of optical guided waves is larger by two figures. The temperature fluctuation induces the change of refractive indices and film thicknesses, which results in the change of the tuning

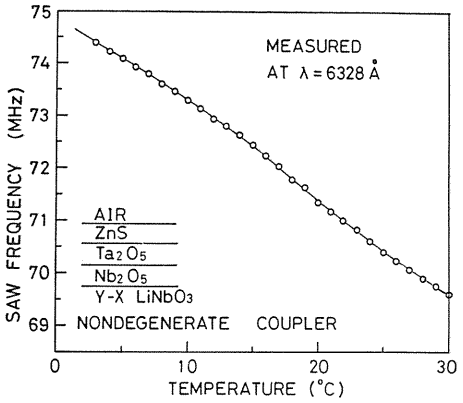

Fig. 6. 2. Tuning SAW frequency as a function of temperature.

Table 6. 1 Refractive indices and their temperature dependence.

MATERIALS		dn/dT ($\times 10^{-5}$/°C)	n (6328 Å)
TiO_2	(n_e)	-7.2	2.865
	(n_o)	-4.2	2.583
$PbMoO_4$	(n_e)	-4.1	2.262
	(n_o)	-7.2	2.386
$LiNbO_3$	(n_e)	+5.3	2.200
	(n_o)	+0.56	2.286
$SrTiO_3$		-5.1	2.39
$Y_3Al_5O_{12}$		+0.73	1.82
$Ga_3Gd_5O_{12}$		+0.52	1.94
ZnSe (polycrystalline)		+9.11	2.59
ZnS (polycrystalline)		+6.35	2.35

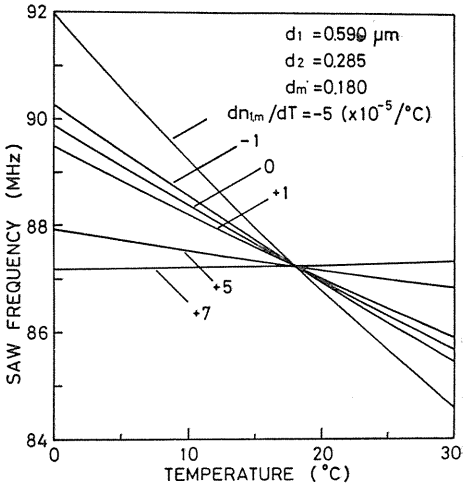

Fig. 6. 3. Shift in tuning SAW frequency.

SAW frequency f. The temperature dependence of the refractive index is tabulated for several high refractive-index materials in Table 6. 1. The temperature coefficients dn/dT of the refractive index are $dn_2/dT=6.35\times10^{-5}℃^{-1}$ and $dn_3/dT=5.3\times10^{-5}℃^{-1}$ for ZnS and $LiNbO_3$, respectively.[44,45] The coefficients of Ta_2O_5 (dn_m/dT) and Nb_2O_5 (dn_1/dT), however, have not been reported. Therefore, several parameters of $dn_{1,m}/dT$ ($=dn_1/dT=dn_m/dT$) are used for evaluation. The coefficients of the linear expansion, which determine the temperature dependence of the film thicknesses, are assumed to be $\alpha=1\times10^{-5}℃^{-1}$ for all the materials. Several high refractive-index materials do not show large difference in the coefficient.

The SAW frequency satisfying the Bragg condition of Eq. (3·3) is calculated as a function of temperature T as shown in Fig. 6. 3. The film thicknesses are determined, according to the device used in Fig. 6. 2, as $d_1=0.590\,\mu$m, $d_2=0.285\,\mu$m and $d_m=0.180\,\mu$m. The gradient becomes large with the increase of the magnitude $|dn_{1,m}/dT|$ with minus sign. This is explained by the fact that the tuning frequency is determined by the discrepancy of the propagation constants between the two modes. The signs of the deviation of k_E and k_O are opposite for the case of $dn_{1,m}/dT\lesssim0$.

The gradient of the curve df/dT is shown as a function of $dn_{1,m}/dT$ around $T=18℃$ in Fig. 6. 4. The measured value in Fig. 6. 2 was $df/dT\fallingdotseq-0.20$MHz/℃. It is found from the comparison with the curve of $d_m=0.180\mu$m that $dn_{1,m}/dT=-3.0\times10^{-5}℃^{-1}$. The temperature dependence of the tuning SAW frequency can be reduced by making the middle layer thin. The device composed of a thinner middle layer by only $0.05\,\mu$m than the fabricated device, that is $d_m=0.13\,\mu$m, has the smaller df/dT that is about 60 percent of the value for $d_m=0.18\mu$m. The noteworthy point in Fig. 6. 4 is that the value df/dT becomes zero at $dn_{1,m}/dT=6.8\times10^{-5}℃^{-1}$.

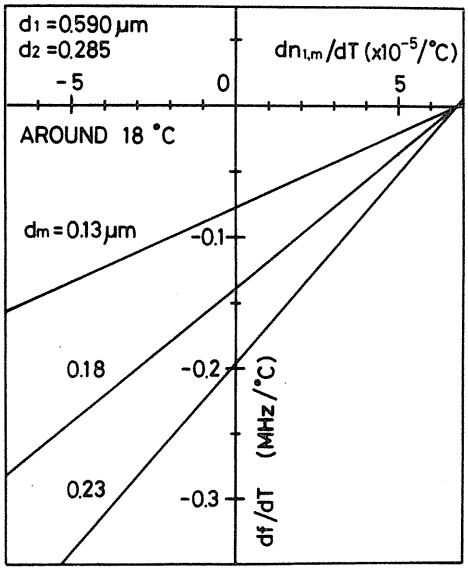

Fig. 6. 4. SAW frequency deviations due to temperature fluctuation.

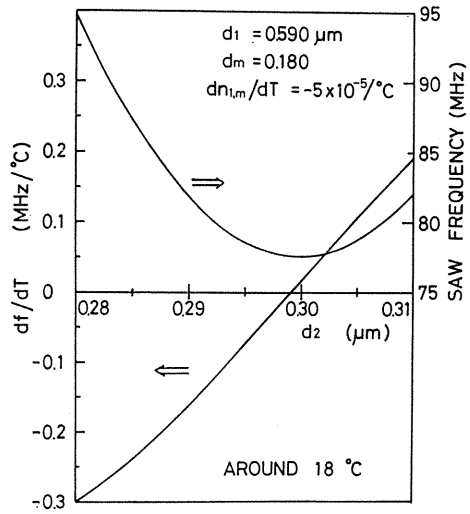

Fig. 6. 5. Tuning frequency and its deviation as a function of the waveguide 2 thickness.

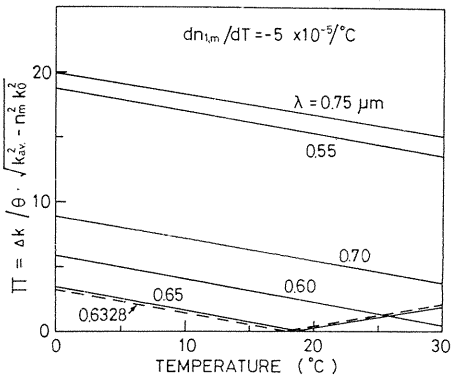

Fig. 6. 6. Temperature dependence of Π at several wavelengths.

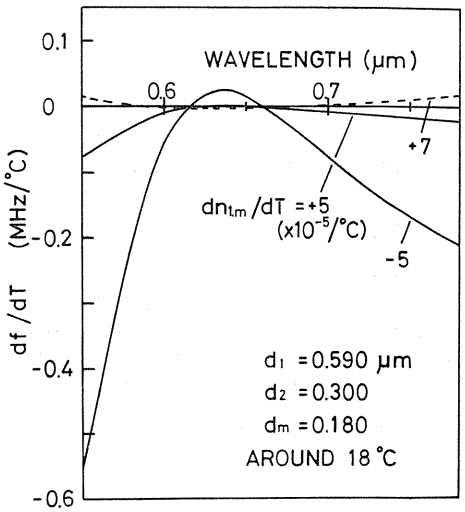

Fig. 6. 7. Wavelength dependence of df/dT.

The dependence of df/dT and the tuning SAW frequency on the film thickness d_2 is shown in Fig. 6. 5, where $dn_{1,m}/dT$ is fixed as $-5\times10^{-5}℃^{-1}$. The waveguides become degenerate for $d_2=0.300\,\mu$m. By calculation of Eq. (2·1), it is shown that the separating branches act as a mode splitter when $d_2\lesssim0.2998\,\mu$m and $d_2\gtrsim0.3008\,\mu$m. Therefore, the device with $d_2\fallingdotseq0.299\,\mu$m shows almost temperature independence and its branches act as a mode splitter. The temperature-independent properties, however, are realized only around a specific optical wavelength of $\lambda_0=6328$Å. The temperature dependence of the value Π is shown in Fig. 6. 6 for different optical wavelengths. The dashed curve shows the dependence at λ_0 and becomes zero at $T=18℃$ where the waveguides support the degenerate modes. The device is operated as the nondegenerate one for $\lambda\lesssim0.59\,\mu$m and $\lambda\gtrsim0.68\,\mu$m in the temperature range of $T\lesssim30℃$. The wavelength dependence of df/dT is shown in Fig. 6. 7. The value df/dT is small around λ_0. The curves for $dn_{1,m}/dT=\pm5$ and $+7\times10^{-5}℃^{-1}$ indicate that the temperature independence over a wide wavelength range is realized by using the materials with $dn_{1,m}/dT=6.8\times10^{-5}℃^{-1}$. It is concluded that the temperature-independent device over a wide wavelength range can be realized when the materials of the two waveguides have almost the same value of dn/dT. When the device is used in a narrow wavelength range, the device with nearly degenerate waveguides can be slightly temperature-dependent.

6. 4. *Experiments of Small Temperature-Dependent Devices*

In order to verify the theoretical results, the temperature dependence was measured in a nearly degenerate device which is used in Section 4. 2. The control frequency was measured with a temperature as shown in Fig. 6. 8. The value of df/dT is almost zero around $T=11℃$ and 0.02 MHz/℃ around $T=18℃$. In the range $T\gtrsim20℃$, the separating branch is considered to have acted as a mode splitter. In the range of $T\lesssim20℃$, however, the branch acted as part of a power divider and part of a mode splitter.

As an example of another small temperature-dependent device, a Ti-diffused

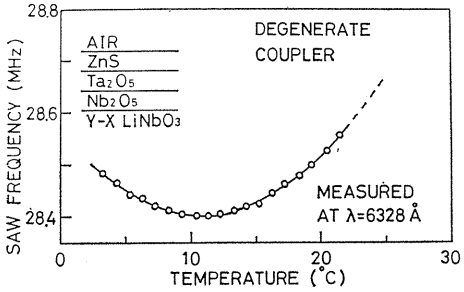

Fig. 6. 8. Tuning frequency in a nearly degenerate device.

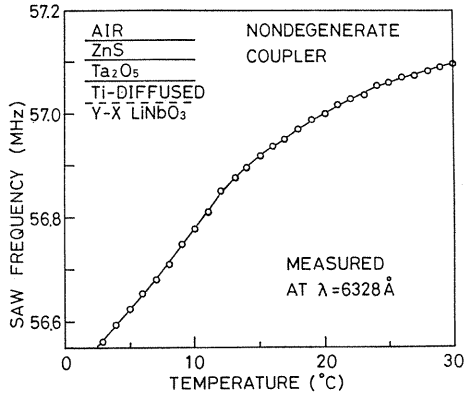

Fig. 6. 9. Tuning frequency in a nondegenerate device with Ti-diffused waveguide.

waveguide was used as waveguide 1 instead of Nb_2O_5. The value dn_1/dT is expected to have 5.3×10^{-5}℃$^{-1}$. The propagation constants of the two modes were $k_E=2.218\times10^7$m^{-1} and $k_O=2.208\times10^7$m^{-1} in the coupling region of $d_m=0.15$ μm. The waveguide 2 is thicker than that for degenerate waveguides. The value Π is estimated as 6. The temperature dependence of the tuning frequency is shown in Fig. 6. 9. The value of df/dT around $T=18$℃ is $+0.02$MHz/℃. This value is about one tenth compared with the previous nondegenerate device as shown in Fig. 6. 2. These measured data confirm the theoretical results. The temperature dependence due to the limit of the material selection can be reduced by using the other overlaid film.[43]

7. SAW Strain Distribution in Layered Media

7. 1. Introduction

To improve the A-O interaction efficiency, it is necessary to investigate both acoustic strain distributions in the films and A-O figures of merit of the film materials. Crystals suitable for bulk A-O devices are not necessarily suitable for waveguide-type devices. In A-O devices, the strain distributions in the waveguides have been investigated to achieve high A-O interaction efficiency in several device configurations with a single waveguide.[46,47] Further, the interaction efficiency has been improved by using an overlay film.[48] In this chapter, the relation between the spatial distributions of strain and the elastic properties of multilayered films is theoretically studied.[49]

7. 2. Relation between Elastic Properties and Strains

The configuration of a SAW propagation medium used in the theoretical analysis is shown in Fig. 7. 1. The optical-waveguide films are assumed to be isotropic, because deposited films are generally amorphous or polycrystalline. The thicknesses of films 1 and 2 are h_1 and h_2, respectively. By solving equations of state and

motion, the SAW velocity and acoustic strains are calculated.[49] The acoustic power is assumed to be 1 watt with 1 mm beam width. The wavelength is assumed to be 50 μm in the numerical evaluation of the absolute magnitude of the strains.

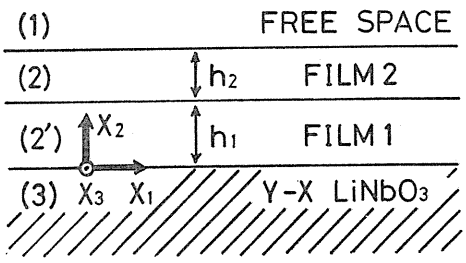

Fig. 7. 1. Configuration of SAW propagation medium.

In isotropic solid materials, two independent elastic constants, c_{11} and c_{44}, characterize the elastic properties. Instead of these two constants, two velocities of the longitudinal wave $\hat{v}_L(=\sqrt{c_{11}/\rho})$ and the degenerate shear waves $\hat{v}_S(=\sqrt{c_{44}/\rho})$ can characterize the elastic properties, where ρ is the mass density. Here, we consider TeO_2 as the film material. The material constants for $LiNbO_3$ and TeO_2 crystals are quoted from refs. 50 and 51. Although TeO_2 crystals belong to a tetragonal system, the following physical constants are used for the amorphous films. The dielectric constant $\varepsilon_{11}=21.2\varepsilon_0$ and the mass density $\rho=5.99\times10^3$kg/m^3 are used for ε_{11} and ρ of the amorphous films, respectively. The elastic constants of the films, c_{11} and c_{44}, are varied around the value of the TeO_2 single crystal.

First, we consider the SAW in the medium of one film of thickness h on the substrate. The parameters $\hat{v}_S$ and $\hat{v}_L$ are assumed to be 2.123km/s and 4.189km/s, respectively, which correspond to the velocities of the wave propagating in the Z axis in the X-Z plane. Mode dispersion curves of the phase velocity are shown in

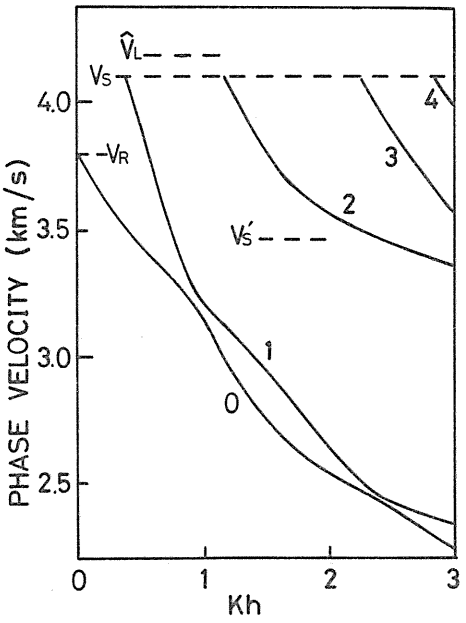

Fig. 7. 2. Dispersion curves of phase velocity.

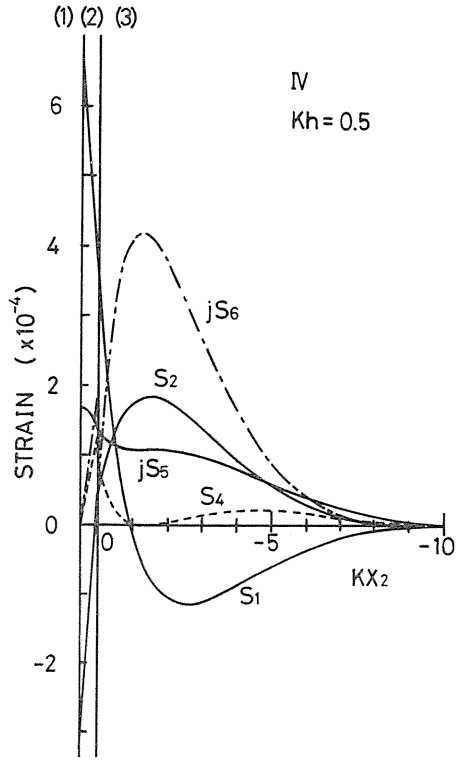

Fig. 7. 3. Strain distributions for $Kh=0.5$

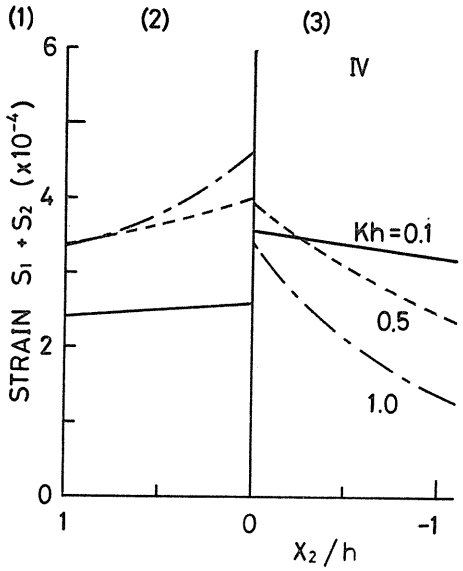

Fig. 7. 4. Strain S_1+S_2 near film for $Kh=0.1$, 0.5 and 1.0.

Fig. 7. 2, where K is the propagation constant of the SAW. The symbols v_S and v_S' denote the phase velocities of shear waves which differ in polarization; v_R is that of a Rayleigh wave without a film. In the range $Kh \lesssim 0.9$ and $Kh \gtrsim 2.4$, the lowest and the first modes are related to Rayleigh and Love waves, respectively. This relation is reversed in the range $0.9 \lesssim Kh \lesssim 2.4$. As for higher modes in $Kh \lesssim 3$, the 2nd and 3rd modes are Rayleigh and Love modes, respectively.

The distributions of strains S_i at $Kh=0.5$ are shown in Fig. 7. 3. There exist distribution discontinuities for S_2, S_4 and S_6 at the interface between the film and the substrate, which are caused by the gradient discontinuity in the mechanical displacement U_2. In isotropic waveguides, the strain component of S_1+S_2 is related to the A-O effect. The distributions of

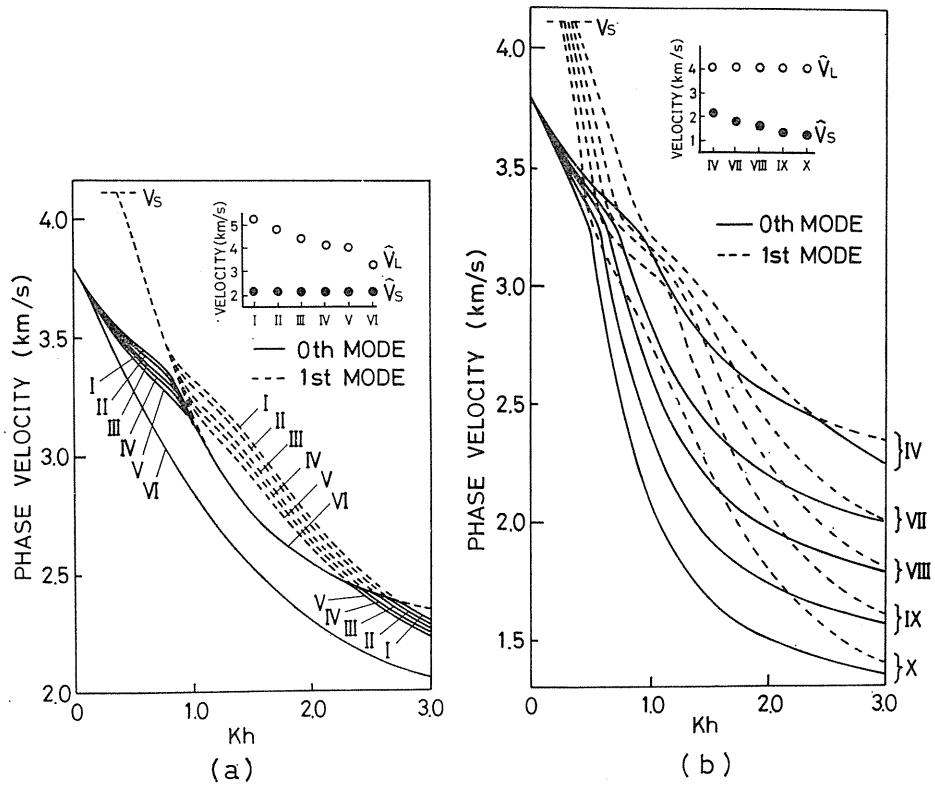

Fig. 7. 5. Dispersion curves of lowest two modes for various values of (a) $\hat{v}_L$ and (b) $\hat{v}_S$.

the summation S_1+S_2 are shown at $Kh=0.1$, 0.5 and 1.0 in Fig. 7. 4. The strains S_1+S_2 are distributed almost uniformly in the film for these small values of Kh.

In order to investigate the relation between the elastic properties of films and the strain distributions, the two parameters $\hat{v}_S$ and $\hat{v}_L$ of the film material are changed around the value discussed above. Figure 7. 5 shows the dispersion curves for the lowest two modes for several values of $\hat{v}_S$ and $\hat{v}_L$. The distributions of S_1+S_2 for several cases Ⅲ, Ⅴ, Ⅵ and Ⅹ are shown in Fig. 7. 6. The amplitude S_1+S_2 in the film changes over the range $1\times10^{-4}\sim5\times10^{-4}$, though the amplitude in the substrate has almost the same value of about 3.5×10^{-4} near the film-substrate interface.

In the next step, the values $\hat{v}_S$ and $\hat{v}_L$ were changed at a constant ratio $\hat{v}_S/\hat{v}_L=0.5$. The dispersion curves and the strain distributions are shown in Fig. 7. 7. Since the acoustic power concentration in the film changes for these cases, the strain in the substrate changes a little. The amplitude of the strains does not differ in the three cases over such a wide range as

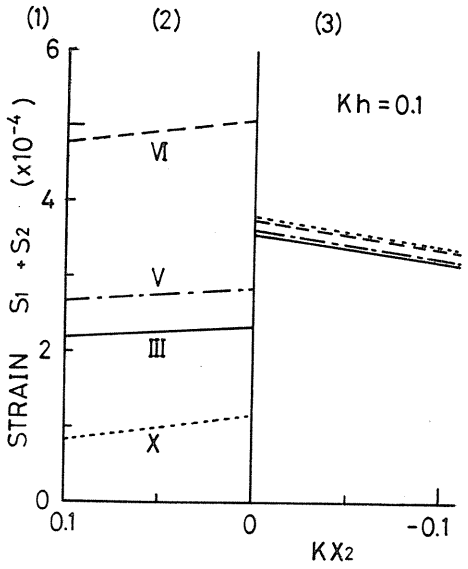

Fig. 7. 6. Strain S_1+S_2 near film for cases Ⅲ, Ⅴ, Ⅵ and Ⅹ.

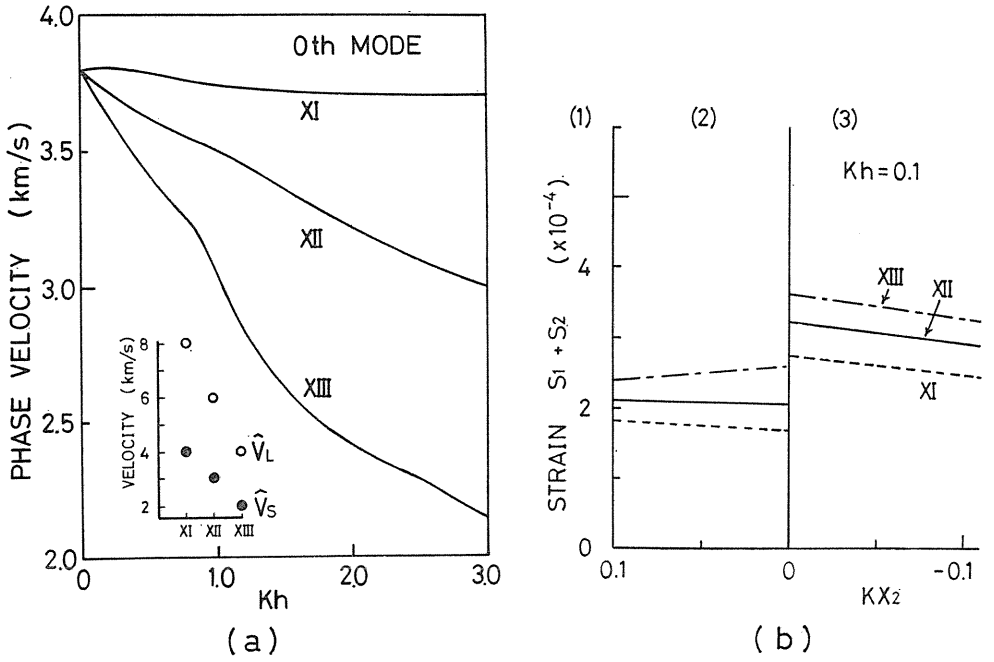

Fig. 7. 7. (a) Dispersion curves and (b) strain S_1+S_2 for the cases of $\hat{v}_S/\hat{v}_L=0.5$.

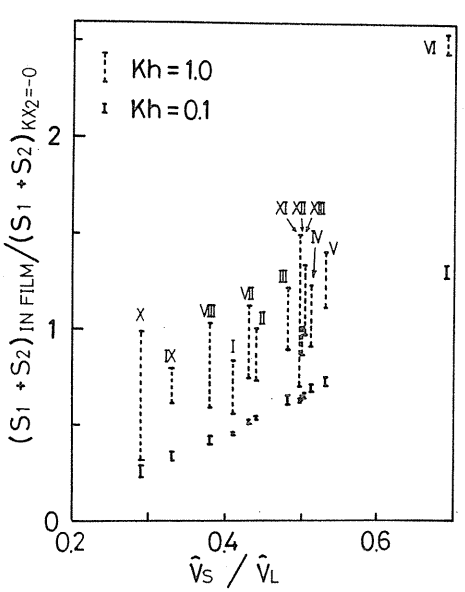

Fig. 7. 8. Relations between $\hat{v}_S/\hat{v}_L$ and S_1+S_2 in the film.

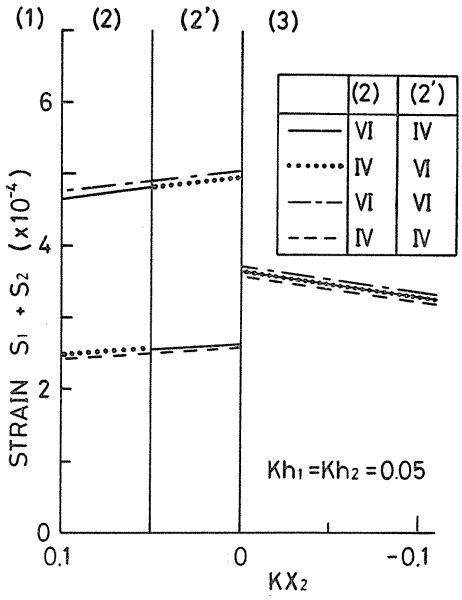

Fig. 7. 9. Strain S_1+S_2 in two-layere films.

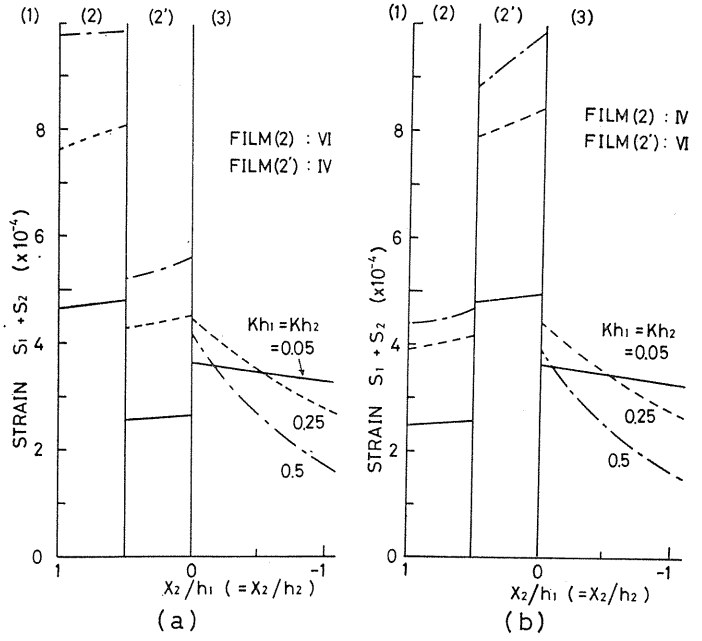

Fig. 7. 10. Strain S_1+S_2 (a) for films 1 and 2 of materials IV and VI, and (b) for films of VI and IV, respectively.

in the cases in Fig. 7. 6.

From a comparison of the strain amplitude in the film for the thirteen cases, it follows that the amplitude of S_1+S_2 in the film increases as the ratio $\hat{v}_S/\hat{v}_L$ increases. Figure 7. 8 shows this relation. The strains are distributed uniformly over the film for values of Kh as small as 0. 1. For $Kh=1.0$, the strain distributions are almost uniform except for the cases Ⅷ, Ⅹ and Ⅺ. However, the strains increase with $\hat{v}_S/\hat{v}_L$ for all cases. Most practical A-O devices have been operated at $Kh\lesssim 1$.

As the final step, we investigate the strains in a medium consisting of two-layered films on a substrate. Figure 7. 9 shows the strain distributions near the films. The solid curve shows the distribution for the case where the materials of films 1 and 2 are Ⅳ and Ⅵ, respectively. The strains for the case in which the two films are of the same materials are also shown. It is found that the strain S_1+S_2 in each film has almost the same amplitude as the strain for the case of one film, even in the layered medium. Figure 7. 10(a) shows the distributions for $Kh_1=Kh_2=0.05$, 0. 25 and 0. 5, where films 1 and 2 are of materials Ⅳ and Ⅵ, respectively. The opposite case of this combination is shown in Fig. 7. 10(b). Even at $Kh_1+Kh_2=1.0$, the distribution has a different amplitude in each film.

7. 3. Evaluation of Elastic Properties of Films

In order to apply the above results to A-O devices, the elastic properties of thin films must be investigated. As a first step, since the velocities of the Love mode are almost independent of $\hat{v}_L$, the velocity $\hat{v}_S$ is determined by comparing the measured values of the velocities of the Love mode with the calculated dispersion curves as shown in Fig. 7. 5(b). Next, the measured velocities of the Rayleigh mode are compared to calculated curves such as those shown in Fig. 7. 5(a). Thus,

Table 7. 1 Physical constants.

MATERIALS	n	$\hat{v}_S/\hat{v}_L$	p_{12}
TeO_2	n_e 2.412 n_o 2.260	0.191 ∿ 1.092	$p_{12}=0.187$
$PbMoO_4$	n_e 2.262 n_o 2.386	0.388 ∿ 0.540	$p_{12}=0.24$
TiO_2	n_e 2.875 n_o 2.583	0.337 ∿ 0.842	$p_{12}=0.172$
α-ZnS	n_e 2.356 n_o 2.351	0.423 ∿ 0.518	$(p_{11}-p_{12})/2=0.019$ (β-ZnS: $p_{12}=-0.01$)
$SrTiO_3$	2.39	0.569 ∿ 0.624	$p_{12}=0.272$
$LiNbO_3$	n_e 2.200 n_o 2.286	0.495 ∿ 0.625	$p_{12}=0.063$
$LiTaO_3$	n_e 2.180 n_o 2.175	0.551 ∿ 0.670	$p_{12}=0.0804$
ZnO	n_e 2.005 n_o 1.988	0.466 ∿ 0.513	$(p_{11}-p_{12})/2=0.046$

the elastic properties such as $\hat{v}_L$ and $\hat{v}_S$ can be obtained by measuring the velocities at several points of Kh.

We survey several waveguide materials in regard to $\hat{v}_S/\hat{v}_L$ and the photoelastic constant p_{12} as shown in Table 7. 1. The values of $\hat{v}_S/\hat{v}_L$ were calculated from the elastic constants of the single crystals.[52] The values $\hat{v}_S/\hat{v}_L$, except for those of TeO_2 and TiO_2, do not vary over such a wide range. It is found that $SrTiO_3$ has potential for use as a highly efficient A-O waveguide. On the other hand, ZnS is estimated to be a low efficient A-O waveguide. Therefore, a device consisting of these two materials will provide high A-O control efficiency.

8. SAW Waveguide

8. 1. Introduction

SAW waveguides have been studied for possible use in signal processing.[53] Effective A-O interaction in waveguide-type collinear A-O devices is realized by using narrow SAW waveguides. The switching SAW power can be reduced to less than one-tenth by employing the SAW waveguide. On integration of A-O devices. SAW waveguides are indispensable for a high integration density. In this chapter, Ta_2O_5 strip waveguides are investigated for use in A-O devices[54~56].

8. 2. Waveguide Structure

Cross-sections of SAW waveguides including optical 3-D and slab waveguides are illustrated in Fig. 8. 1(a) and (b), respectively. Three kinds of SAW waveguides, that is, $\Delta v/v$, strip and slot waveguides, are considered to be suitable for A-O devices. In $\Delta v/v$ waveguides, a transparent conducting film or a thin buffer underlayer have to be employed to elude optical propagation loss. In the slot waveguide, the film material is "faster" than that of the substrate. The presence of the film increases the SAW velocity. Thin films of Al_2O_3[54] or Ti-diffusion[57] can construct slot waveguides. In the strip waveguide, the film itself consists of "slower" material. When a buffer layer is not placed between the optical and acoustic waveguide films, the strip film must be transparent with a refractive index smaller than that of the

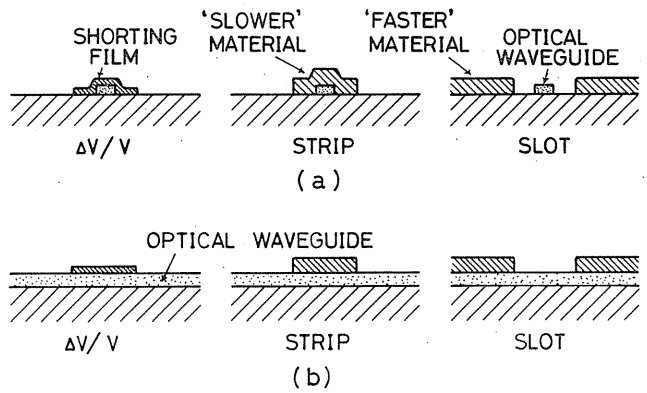

Fig. 8. 1. Cross-sections of SAW waveguides; (a) with an optical 3-D waveguide, (b) with an optical slab waveguide.

supporting optical waveguide. Here, we investigate Ta_2O_5 strip waveguides in comparison with $\Delta v/v$ waveguides. The velocity decrease due to Ta_2O_5 films was measured on $LiNbO_3$ substrates. When the velocity decrease is expressed as $v_f - v_{f0} = \delta \cdot \Omega$, where Ω is the acoustic angular frequency, the value δ for various propagation directions on Y- and Z-cut $LiNbO_3$ substrates was measured as shown in Fig. 8. 2. The velocity v_{f0} is the SAW velocity without films. The velocity decrease $v_f - v_{f0}$ was measured from the amount of the center frequency shift in the IDT. The SAW strip waveguides are found to be composed of a Ta_2O_5 film on both Y- and Z-cut $LiNbO_3$ substrates.

The guided wave velocity and the insertion loss between two IDTs were measured. The strip waveguide between the two IDTs (10mm propagation) reduced the insertion loss as shown in Fig. 8. 3(a). The insertion loss except for the electromechanical coupling loss is about 18dB, which is improved to be 9dB by using the strip waveguide. The insertion loss in the waveguide placed on a Nb_2O_5 slab optical film is shown in Fig. 8. 3(b). The electro-mechanical coupling efficiency is reduced in this device because of the existence of the Nb_2O_5 film. It is found that the guiding effect in the Ta_2O_5 strip waveguide was not reduced by the slab film under the strip.

The experimental results in these Ta_2O_5 strip waveguides are summarized with the theoretical values in Table 8. 1, compared with $\Delta v/v$ waveguides. The velocity was calculated by a method presented by Schmidt and Coldren.[55,58] In the $\Delta v/v$ waveguides the film thickness represents the underlaid Ta_2O_5 film thickness. The phase velocity v_p was measured as a ratio normalized by the velocity in a reference channel.[55,59] The improvement of insertion loss in Ta_2O_5 strip waveguides is larger than that in $\Delta v/v$ waveguides. The propagation loss is described by the experimental results obtained in the next section.

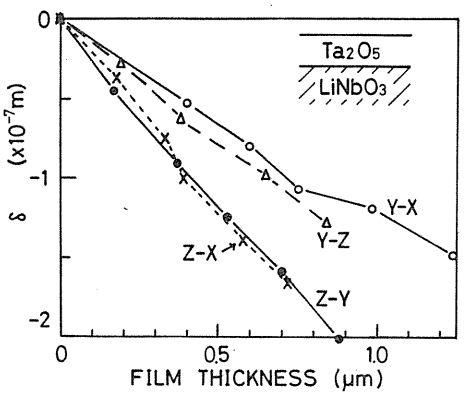

Fig. 8. 2. The value δ as a function of the Ta_2O_5 film thickness.

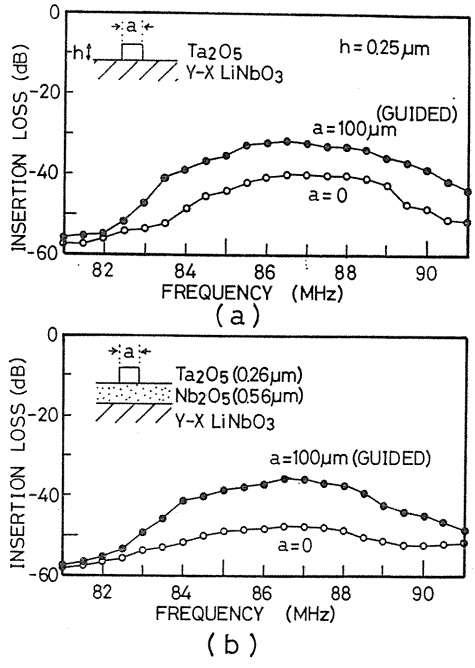

Fig. 8. 3. Insertion loss between two IDTs in Ta_2O_5 strip waveguides; (a) on substrate alone and (b) on Nb_2O_5 film.

Table 8. 1 Normalized velocity and losses ($f \simeq 86$ MHz, $a = 100\ \mu$m).

	FILM (μm) THICKNESS	$(V_P - V_r)/V_r$ ($\times 10^{-3}$) MEASURED	CALCULATED	IMPROVEMENT OF INSERTION LOSS(dB)	PROPAGATION LOSS (dB/cm)
$\Delta V/V$ Al / Ta_2O_5 / Y-X $LiNbO_3$	0	3.47	3.60	7.0	< 1
	0.32	2.57	2.85	6.5	2.5
	0.55	2.39	2.30	5.0	4
STRIP Ta_2O_5 (h_2) / Nb_2O_5 (h_1) / Y-X $LiNbO_3$	$h_1 = 0$ $h_2 = 0.25$	-4.68	-2.40	9.0	1
	$h_1 = 0.56$ $h_2 = 0.26$	-4.17	——	12.0	< 1

8. 3. Guided Beam Profiles

The guided beam profiles were measured by an optical probing method.[60] The spot size of 1mW He-Ne laser had the diameter of about 40 μm at the surface. The SAW was confined in the Ta_2O_5 waveguide as shown in Fig. 8. 4. The R. F. electric power of 100 mW was fed into the IDT. Interference effects in the Ta_2O_5 film reduced the diffracted intensity by one half as shown in the zero-order reflected shape.[61] It is found from Fig. 8. 4(b) that the slab film under the strip does not reduce the energy confinement in the waveguide. The relative peak in-

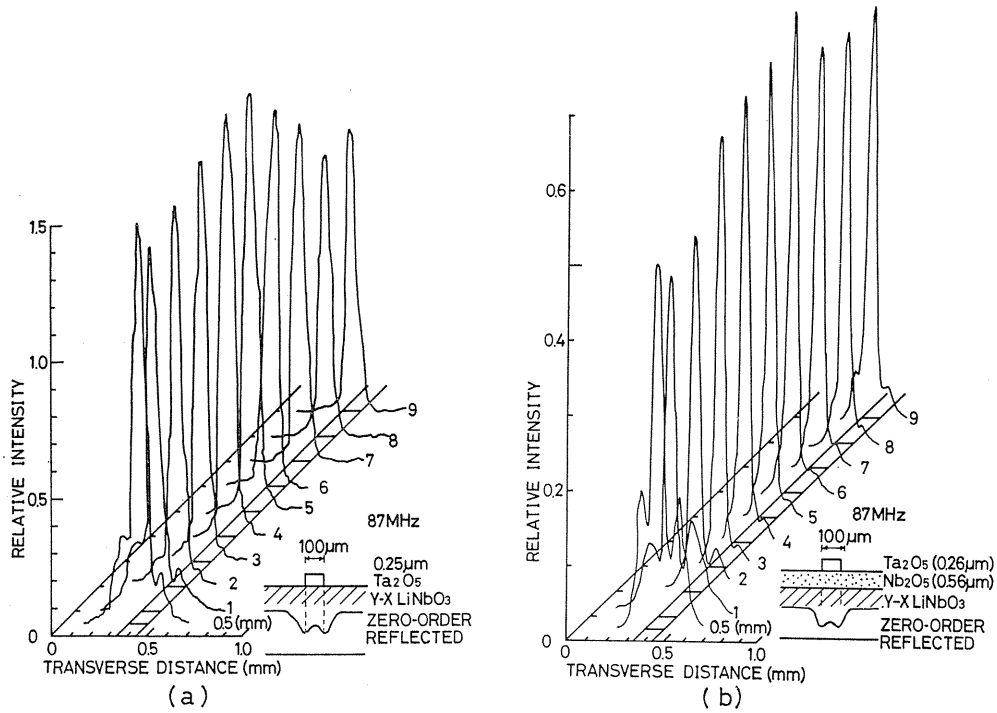

Fig. 8. 4. Beam profiles in Ta_2O_5 strip waveguide placed (a) on substrate alone and (b) on Nb_2O_5 film.

tensity for the strip waveguides is plotted as a function of the propagation distance in Fig. 8. 5. The propagation loss of the SAW, excited by a 100 μm-width IDT without waveguides, is approximately 28dB/cm as shown by the dotted line. The intensity increase around the propagation distance of 5mm is a result of interference between guided and non-guided waves. The propagation loss is equal or less than 1 dB/cm.

The beam profiles in the Al $\Delta v/v$ waveguide on a Ta_2O_5 slab film were obtained as shown in Fig. 8. 6. As known from the zero-order reflected profile, the obtained profiles are much more confined than the real displacement profiles. The peak intensity of the beam profiles for the $\Delta v/v$ waveguides are plotted in Fig. 8. 7. Since the slab film under the Al strip reduces Δv, the guiding effect becomes weaker with increasing the film thickness. The propagation loss for the waveguides exclusive of the coupling loss is summarized in Table 8. 1.

8. 4. Coupling with Focused IDT

In order to realize effective coupling into the narrow waveguide, a focused IDT was employed,[62] whose focal point was adjusted onto the edge of the waveguide as shown in Fig. 8. 8. The focal length and the aperture width of the IDT were 1. 8 mm and 0. 75 mm, respectively. The angle θ was determined 15 degree, considering the substrate anisotropy and

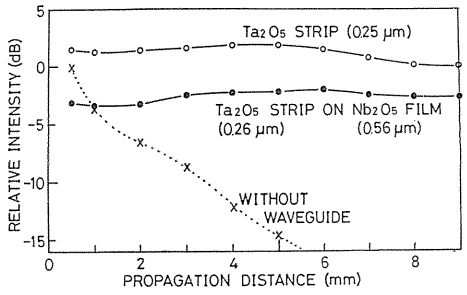

Fig. 8. 5. Relative peak intensity of SAW beam.

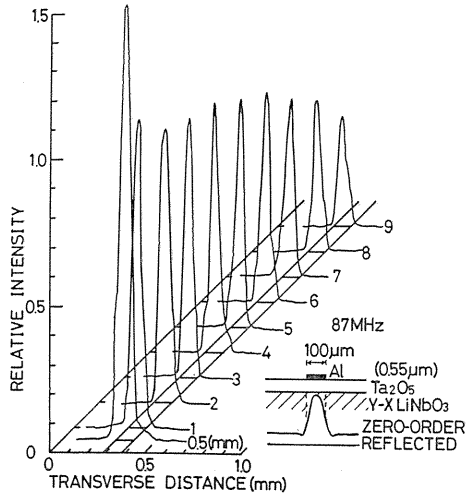

Fig. 8. 6. Beam profiles in Al $\Delta v/v$ waveguide placed on Ta_2O_5 film on substrate.

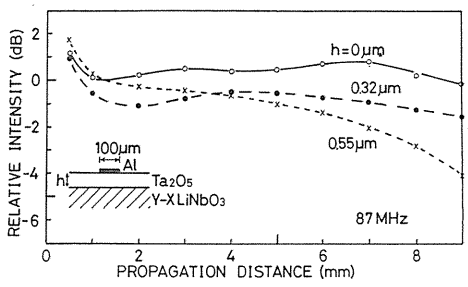

Fig. 8. 7. SAW beam propagation in $\Delta v/v$ waveguide.

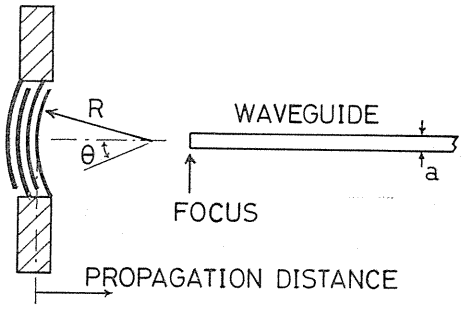

Fig. 8. 8. Diagram of curved IDT with strip waveguide.

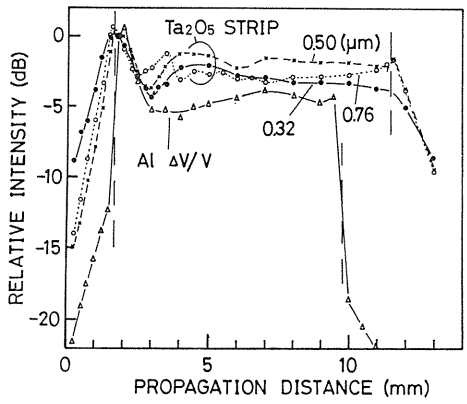

Fig. 8. 9. SAW beams excited by focused IDT.

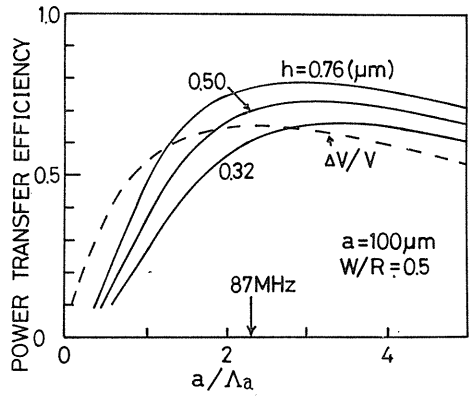

Fig. 8. 10. Power transfer efficiency into strip and $\Delta v/v$ waveguides.

a critical angle in the strip waveguide. The focal spot size was measured to be about 100 μm at 87 MHz. The relative peak intensity of the SAW beam is plotted for a Ta_2O_5 strip with several film thicknesses in Fig. 8. 9, where the intensity is normalized at the incident point in the waveguide. The decrease around 3 mm propagation is caused by the interference between guided and non-guided waves. The coupling loss is compared to the theoretical values shown in Fig. 8. 10.[62] The coupling efficiency depends on a/Λ_a, where Λ_a is the SAW wavelength in free surface. The calculated coupling losses at 87 MHz are 1. 1, 1. 5 and 2. 2 dB in Ta_2O_5 strip waveguides of $h=0.76$, 0. 50 and 0. 32 μm, which are in fairly good agreement with the experimental results of about less than 2, 2 and 3dB, respectively.

8. 5. Al-Coated Ta_2O_5 Strip Waveguide

The mode confinement in the waveguide decreases as the frequency decreases. Propagation properties at four different frequencies were measured as shown in Fig. 8. 11. The SAWs were excited by an ordinary IDT of 100 μm-width. The propagation loss is about 1dB at the four frequencies. However, the guided beam width spreads rapidly as the frequency decreases, because the velocity decrease due to the existence of Ta_2O_5 film, $v_f - v_s$, reduces in the low frequency range as shown in Fig. 8. 12. In order to obtain stronger confinement in a wider frequency range, an aluminum coated Ta_2O_5 strip waveguide is investigated.[56] The coated Al film additionally decreases the velocity only in the low frequency region as shown by the dashed line of v_s'. Therefore, the cut-off frequency of the higher mode does not greatly decrease. The guided beam width is plotted by theoretical curves in Fig. 8. 13. The beam width at 40MHz was reduced by 200 μm in an Al-coated

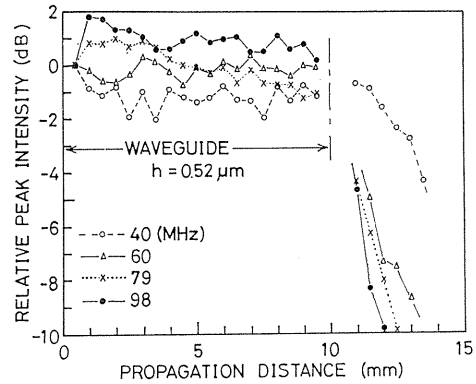

Fig. 8. 11. SAW propagation at four frequencies.

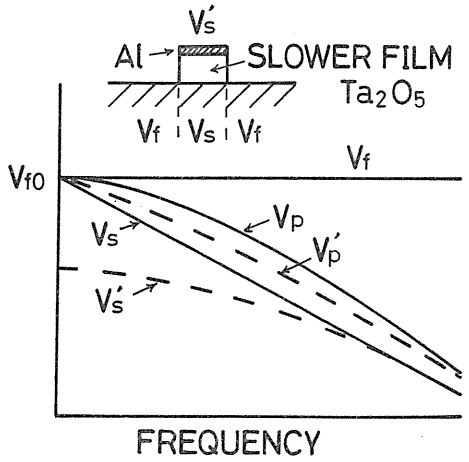

Fig. 8. 12. Velocity dispersion in the strip region (v_s) and in the free surface (v_f). v_p denotes the phase velocity of guided waves. The superscript "′" indicates Al-coated Ta_2O_5.

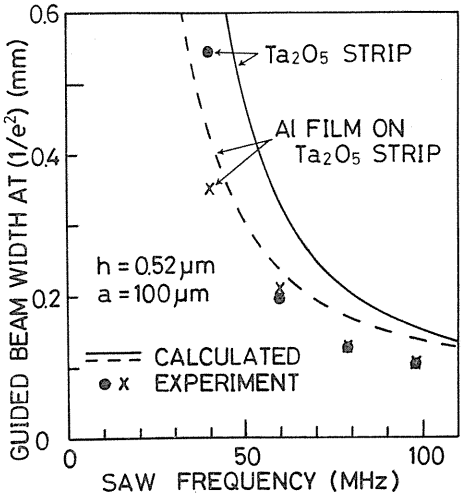

Fig. 8. 13. Guided beam width.

waveguide.

With these waveguides, the A-O interaction efficiency is improved by more than ten times; further, integration of A-O devices becomes possible as discussed in the next chapter.

9. A-O Device Consisting of Channel Waveguides and Its Application to Signal Processing

9. 1. Introduction

In order to integrate the A-O device and to connect such a device with fibers, it is indispensable to confine optical waves in channel waveguides. By using optical channel waveguides and SAW strip waveguides, the A-O switches are applied to various signal processors. As examples of such processors, a signal exchange device and an accessor for optical communication networks and matrix multiplications in optical computing are described in this chapter.[63,64] Broad-band signal exchange switches and accessors are indispesable for optical fiber networks.[65~68] Matrix multiplications have been investigated for various integrated optical devices so far.[69,70]

9. 2. Device Description

A switching element consisting of A-O channel waveguides is illustrated in Fig. 9. 1. The two optical waveguides are multilayered over the interaction region. Therefore, the coupling strength depending on the separating layer thickness is easily controlled. The switching mechanism is the same as that in slab-waveguide devices. As a lower straight waveguide, Ti-diffused or proton-exchanged single-

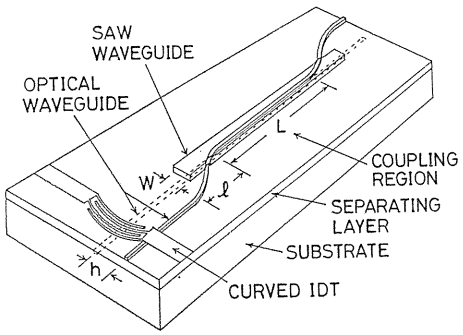

Fig. 9. 1. Channel-waveguide switch.

mode channel waveguides are suitable. The upper curved waveguide is realized with a ridge waveguide. The width of these optical waveguides is 2~4 μm.[71]

One-way and two-way switching for wavelength-multiplexed optical signals are controlled by frequency-multiplexed SAWs as shown in Fig. 9. 2. Switching properties in a device consisting of channel waveguides are estimated from the experimental results with the slab-waveguide device as discussed in Chapters 4 and 5. The results are summarized in Table 9. 1.

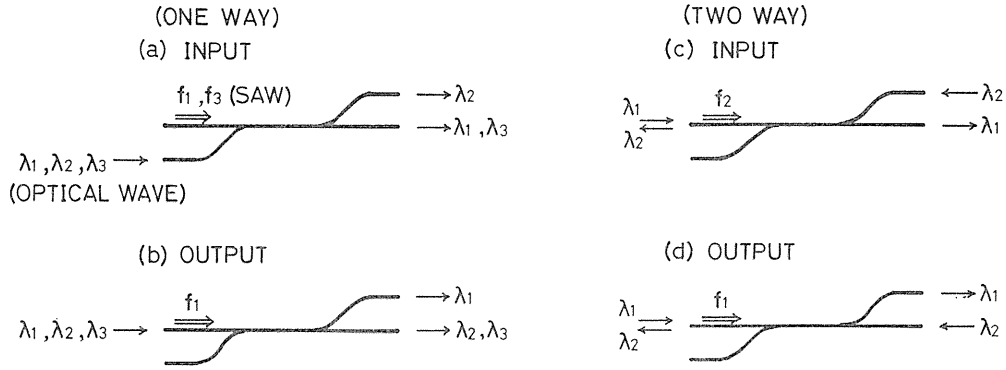

Fig. 9. 2. Wavelength-selective control for multiplexed signals.

Table 9. 1 Estimated properties of a channel waveguide device.

INTERACTION LENGTH	8 mm
SAW FREQUENCY	75 MHz
SAW WAVEGUIDE WIDTH	100 μm
REQUIRED SAW POWER	6 mW
SWITCHING SPEED	2 μS
PASS BANDWIDTH	11 Å

9. 3. Optical Exchange Switches and Accessors

Signal exchange switches in optical communication systems are composed of integrated A-O switches. The A-O switches are especially useful in multi-wavelength systems, compared to electro-optic switches.[67] Figure 9. 3 shows a 3×3 exchange device with nine integrated switches. Since the multiplex number of the wavelength is three, optical signals are exchangeable in nine channels. Optical waves of wavelength λ_k are switched with switch S_{ij} by the interacting SAW of the frequency f_{jk}, where i, j, k=1, 2, 3. A set of series switches, S_{i1}, S_{i2} and S_{i3}, is controlled by SAWs excited by one curved IDT at f_{1k}, f_{2k} and f_{3k}, respectively. The channel number is easily increased by increasing the multiplexing number of the optical wavelength.

Optical accessors in optical communication or data buses are designed in a similar way. Figure 9. 4 shows a six-wavelength two-way accessor connected to a one-bus-fiber. The output switch elements are used for both right and left way

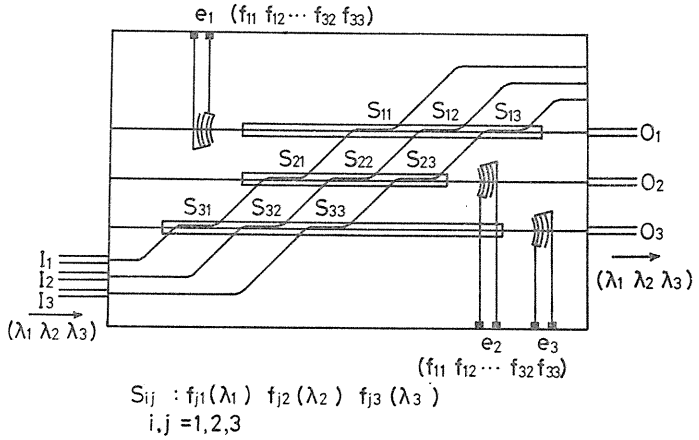

Fig. 9. 3. Signal exchange device.

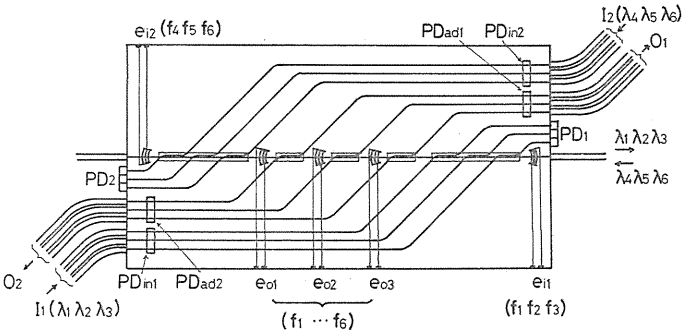

Fig. 9. 4. Two-way accessor.

in common. For example, when the destination of a signal of λ_k is the center of the output terminal O_1. The SAW power at f_k from e_{o2} transmits the signal into the output channel. When the wavelength λ_j is idle, an input signal is transmitted at λ_j from the terminal. The switch is operated by the SAW at f_j. Instead of the three series input switches, the same functions are obtained by one switch and a three-branch optical power divider.[63]

9. 4. Matrix Multiplication

By using A-O switches as modulators, multiplications of the type matrix-vector and matrix-matrix are performed. A matrix-vector multiplication is realized with one A-O modulator as shown in Fig. 9. 5. The vector components, b_1 and b_2, are used to module SAWs of f_1 and f_2, respectively. At time t_1, optical pulses of λ_1 and λ_2 modulated by matrix columns a_{11} and a_{12}, respectively, are coupled in the waveguide. The output signals in λ_1 and λ_2 represent $a_{11}b_1$ and $a_{12}b_2$, respectively. Therefore, a detected optical power corresponds to the summation $a_{11}b_1+a_{12}b_2$ as shown by a time chart in Fig. 9. 6. At time t_2, the next pulses modulated by a_{21} and a_{22} pass through the modulator with the resultant detected output of $a_{21}b_1+a_{22}b_2$. Matrices and vectors having more components are multiplied by

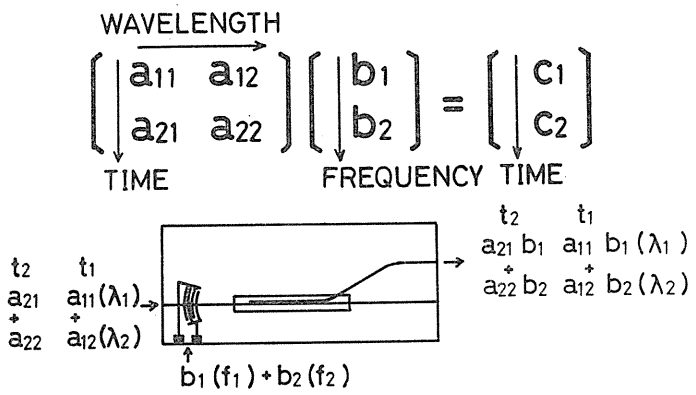

Fig. 9. 5. Matrix-vector multiplication.

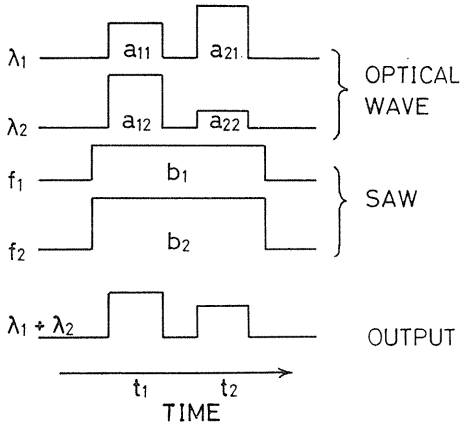

Fig. 9. 6. Time chart of matrix-vector multiplication.

multiplexing optical signals with more wavelengths.

Matrices of 2×2 components are used for an example of matrix-matrix multiplication as shown in Fig. 9. 7. The optical power of the signals is divided into two A-O modulators at a Y-junction. The components $a_{11}b_{11}+a_{12}b_{21}$ and $a_{11}b_{12}+a_{12}b_{22}$ are obtained at time t_1 as the outputs from the two modulators. At time t_2, the other two components, $a_{21}b_{11}+a_{22}b_{21}$ and $a_{21}b_{12}+a_{22}b_{22}$, are obtained. By integrating more A-O modulators and increasing the multiplexing wavelength number, matrices involving more components are multiplicated in a similar

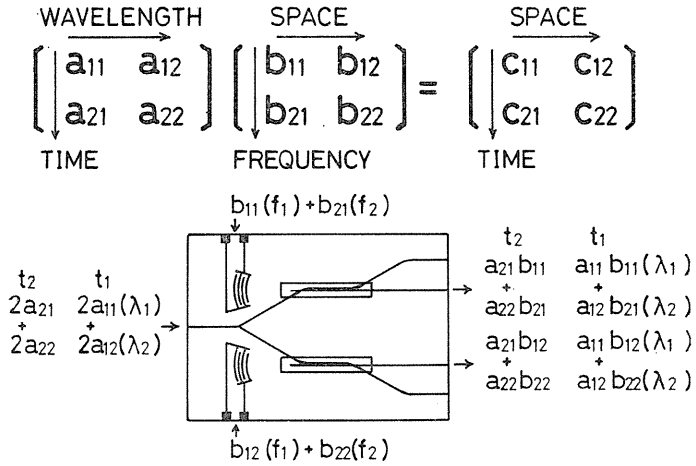

Fig. 9. 7. Matrix-matrix multiplication.

manner. In these processors, very high speed calculation is possible, because the processing time depends only on the periodic time of the optical pulses.

10. Conclusion

Tunable optical wavelength separators and filters were investigated for use in wavelength-division-multiplex systems. It was found from the discussion in this paper that one of the important features of this device exists in the independent control for several optical signals at different wavelengths by frequency-multiplexed SAWs. By using these characteristics, various kinds of signal processors are realized.

The obtained results are summarized as follows:

1) Optical switching was obtained in both degenerate and nondegenerate devices due to mode conversion between optical even and odd modes by A-O interaction. It was shown that the separating branch acts as a power divider and as a mode splitter in the degenerate and nondegenerate devices, respectively. The nondegenerate device showed better characteristics for practical use than the degenerate one.

2) These two kinds of switches were experimentally confirmed with the devices consisting of $ZnS/Ta_2O_5/Nb_2O_5$ multilayered films on Y–X $LiNbO_3$ substrates.

3) Wavelength-selective control for optical waves of 6328 Å and 7791 Å was demonstrated with a tuning sensitivity of $3.4\times10^{-3}MHz^{-1}$ and a half-power bandwidth of 27 Å.

4) Small temperature-dependent devices were obtained by composing the two waveguides using the materials with similar temperature properties.

5) In order to improve the A-O interaction efficiency, the strain fields of the SAW were theoretically studied. Required properties for the optical waveguide material were clarified.

6) Three-dimensional strip waveguides for the SAW were found to be composed of Ta_2O_5 film with excellent mode confinement.

7) As applications to signal processing, signal exchange devices in optical communication system and matrix multiplications in optical computing were proposed.

As discussed in Chapter 9, three-dimensional optical waveguides are indispensable for the practical use and for the integration of the device. The devices consisting of such channel waveguides are under investigation. In order to realize high A-O interaction efficiency and temperature independence, further study on the most suitable composite materials are needed.

References

1) E. G. Lean, J. M. White and C. D. Wilkinson: "Thin-Film Acousto-Optic Devices", Proc. IEEE, **64**, 5, p. 779 (1976).

2) C. S. Tsai: "Guided-Wave Acoustooptic Bragg Modulators for Wide-Band Integrated Optic Communications and Signal Processing", IEEE Trans. Circuits & Syst., **CAS-26**, 12, p. 1072 (1979).

3) R. C. Alferness: "Guided-Wave Devices for Optical Communication", IEEE J. Quantum Electron., **QE-17**, 6, p. 946 (1981).
4) R. C. Alferness: "Waveguide Electrooptic Modulators", IEEE Trans. Microwave Theory & Tech., **MTT-30**, 8, p. 1121 (1982).
5) H. Ishio, J. Minowa and K. Nosu: "Review and Status of Wavelength-Division-Multiplexing Technology and Its Application", J. Lightwave Technol., **LT-2**, 4, p. 448 (1984).
6) G. Winzer: "Wavelength Multiplexing Components—A Review of Single-Mode Devices and Their Applications", J. Lightwave Technol., **LT-2**, 4, p. 369 (1984).
7) M. Izutsu, M. Kato and T. Sueta: "A Guided-Wave Acoustooptic Tunable Filter Making Use of Collinear TE-TM Mode Conversion", Trans. IECE Japan, **E63**, 7, p. 532 (1980).
8) L. N. Binh, J. Livingstone and D. H. Steven: "Tunable Acousto-Optic TE-TM Mode Converter on a Diffused Optical Waveguide", Opt. Lett., **5**, 3, p. 83 (1980).
9) B. Kim and C. S. Tsai: "Thin-Film Tunable Optical Filtering Using Acoustooptic and Noncollinear Acoustooptic Interaction in $LiNbO_3$ Waveguides", IEEE J. Quantum Electron., **QE-15**, 7, p. 642 (1979).
10) R. C. Alferness: "Efficient Waveguide Electro-Optic TE-TM Mode Converter with Low Drive Voltage", Opt. Lett., **5**, 11, p. 473 (1980).
11) R. C. Alferness and L. L. Buhl: "Tunable Electro-Optic Waveguide TE-TM Converter/Wavelength Filter", Appl. Phys. Lett., **40**, 10, p. 861 (1982).
12) R. C. Alferness and R. V. Schmidt: "Tunable Optical Waveguide Directional Coupler Filter", Appl. Phys. Lett., **33**, 2, p. 161 (1978).
13) N. Chubachi: "Interaction of Optical Guided Waves with Elastic Surface Waves", The Journal of the Acoustical Society of Japan, **30**, 10, p. 569 (1974).
14) T. Suhara, Y. Handa, H. Nishihara and J. Koyama: "Monolithic Integrated Micrograting and Photodiodes for Wavelength Demultiplexing", Appl. Phys. Lett., **40**, 2, p. 120 (1982).
15) T. Suhara, T. Shiono, H. Nishihara and J. Koyama: "An Integrated-Optic Fourier Processor Using an Acoustooptic Deflector and Fresnel Lenses in an As_2S_3 Waveguide", J. Lightwave Technol., **LT-1**, 4, p. 624 (1983).
16) S. Valette, J. Lizet, P. Mottier, J. P. Jadot, P. Gidon and S. Renard: "Integrated-Optical Circuits Achieved by Planar Technology on Silicon Substrates: Application to the Optical Spectrum Analyser", IEE Proc., **131**, pt. H, 5, p. 325 (1984).
17) T. Kondo, Y. Miyazaki and Y. Akao: "Optical Tunable Switched Directional Couplers Consisting of Two Thin-Film Waveguides Using Surface Acoustic Waves", Jpn. J. Appl. Phys., **17**, 7, p. 1231 (1978).
18) Y. Miyazaki, N. Goto and Y. Akao: "Optical Switching Properties of Multilayered Thin-Film Optical Tunable Separators and Couplers Using Surface Acoustic Waves", *Proceeding of IEEE Ultrasonic Symposium*, O-5 (San Diego, Calif., USA, 1982).
19) N. Goto, Y. Miyazaki and Y. Akao: "Optical Switching Characteristics in a Multilayered Directional Coupler Using Acousto-Optic Effects by Surface Acoustic Waves", Trans. IECE Japan, **E66**, 1, p. 21 (1983).
20) N. Goto, Y. Miyazaki and Y. Akao: "Optical Switching Characteristics in Slightly Nondegenerated Multilayered Couplers Using Acousto-Optic Interaction by Surface Acoustic Waves", Trans. IECE Japan, **E66**, 7, p. 442 (1983).
21) N. Goto, Y. Miyazaki and Y. Akao: "Switching Properties of Optical Guided Waves in Multilayered Thin-Film Tunable Separators by Surface Acoustic Waves", Jpn. J. Appl. Phys., **22**, Supplement 22-3, p. 176 (1983).
22) H. Yajima: "Dielectric Thin-Film Branching Waveguide", Trans. IECE Japan, **57-C**, 9, p. 297 (1974).
23) H. Yajima: 'Dielectric Bypass Waveguide Mode Order Converter", IEEE J. Quantum Electron., **QE-15**, 6, p. 482 (1979).
24) W. K. Burns and A. F. Milton: "Mode Conversion in Planar-Dielectric Separating Waveguides", IEEE J. Quantum Electron., **QE-11**, 1, p. 32 (1975).
25) W. K. Burns and A. F. Milton: "An Analytic Solution for Mode Coupling in Optical

Waveguide Branches", IEEE J. Quantum Electron., **QE-16**, 4, p. 446 (1980).
26) Y. Ohmachi and J. Noda: "$LiNbO_3$ TE-TM Mode Converter Using Collinear Acoustooptic Interaction", IEEE J. Quantum Electron., **QE-13**, 2, p. 43 (1977).
27) K. Yamanouchi, K. Higuchi and K. Shibayama: "High Efficiency TE-TM Mode Converter by Acousto-Optic Interaction", Trans. IECE Japan, **J61-C**, 1, p. 47 (1978).
28) N. Goto, Y. Miyazaki and Y. Akao: "Filtering Properties of Multilayered Thin-Film Optical Tunable Couplers Using Surface Acoustic Waves", Trans. IECE Japan, **E64**, 9, p. 602 (1981).
29) N. Goto, Y. Miyazaki and Y. Akao: "Characteristics of Multilayered Thin-Film Optical Tunable Separators Using Surface Acoustic Waves", Jpn. J. Appl. Phys., **20**, Supplement 20-3, p. 283 (1981).
30) N. Goto, Y. Miyazaki and Y. Akao: "Tunable Filtering Characteristics of Multilayered Optical Couplers Using Surface Acoustic Waves", Jpn. J. Appl. Phys., **21**, 11, p. 1611 (1982).
31) M. Nakahara, Y. Miyazaki and Y. Akao: "R. F. Sputtering Fabrication of Multi-Layer Thin Film Type Tunable Optical Coupler Using Surface Acoustic Wave", *Proceedings of 2nd Meeting on Ferroelectric Materials and Their Applications*, E-6, p. 49 (1979).
32) D. H. Hensler, J. D. Cuthbert, R. J. Matin and P. K. Tien: "Optical Propagation in Sheet and Pattern Generated Films of Ta_2O_5", Appl. Opt., **10**, 5, p. 1037 (1971).
33) S. Dutta, H. E. Jackson, J. T. Boyd, R. L. Davis and F. S. Hickernell: "CO_2 Laser Annealing of Si_3N_4, Nb_2O_5, and Ta_2O_5 Thin-Film Optical Waveguides to Achieve Scattering Loss Reduction", IEEE J. Quantum Electron., **QE-18**, 4, p. 800 (1982).
34) S. J. Ingrey, W. D. Westwood, Y. C. Cheng and J. Wei: "Variable Refractive Index and Birefringent Waveguides by Sputtering Tantalum in O_2-N_2 Mixtures", Appl. Opt., **14**, 9, p. 2194 (1975).
35) W. L. Bond: "Measurement of the Refractive Indices of Several Crystals", J. Appl. Phys., **36**, 5, p. 1674 (1965).
36) M. V. Hobden and J. Warner: "The Temperature Dependence of the Refractive Indices of Pure Lithium Niobate", Phys. Lett., **22**, 3, p. 243 (1966).
37) R. C. Alferness and J. J. Veselka: "Simultaneous Modulation and Wavelength Multiplexing with a Tunable Ti: $LiNbO_3$ Directional Coupler Filter", Electron. Lett., **21**, 11, p. 466 (1985).
38) N. Goto, Y. Miyazaki and Y. Akao: "Tunable Wavelength-Selective Characteristics of Multilayered Thin-Film Optical Separators Using Surface Acoustic Waves", Jpn. J. Appl. Phys., **23**, 4, p. 410 (1984).
39) N. Goto, Y. Miyazaki and Y. Akao: "Temperature Dependencies of Tunable Thin-Film Optical Separators Using Surface Acoustic Waves", Jpn. J. Appl. Phys., **23**, Supplement 23-1, p. 168 (1984).
40) T. Okoshi and K. Kikuchi: "Frequency Stabilisation of Semiconductor Lasers for Heterodyne-Type Optical Communication Systems", Electron. Lett., **16**, 5, p. 179 (1980).
41) M. Haruna and J. Koyama: "Thermooptic Deflection and Switching in Glass", Appl. Opt., **20**, 19, p. 3461 (1982).
42) S. L. Chen and J. T. Boyd: "Temperature-Independent Thin-Film Optical Waveguide", Appl. Opt., **20**, 13, p. 2280 (1981).
43) N. Goto, Y. Miyazaki and Y. Akao: "Improvement of Temperature Independencies in Multilayered Tunable Optical Separators Using Surface Acoustic Waves", Trans. IECE Japan, **E68**, 10, p. 698 (1985).
44) R. J. Harris, G. T. Johnston, G. A. Kapple, P. C. Krok and H. Mukai: "Infrared Thermooptic Coefficient Measurement of Polycrystalline ZnSe, ZnS, CdTe, CaF_2 and BaF_2, Single Crystal KCl and TI-20 Glass", Appl. Opt., **16**, 2, p. 436 (1977).
45) E. Schneider, P. J. Cressman and R. L. Holman: "Temperature Dependence of the Refractive Index of Strontium Titanate and Prism Coupling to Lithium Niobate Optical Waveguides", J. Appl. Phys., **53**, 6, p. 4054 (1982).
46) H. Sasaki, J. Kushibiki, N. Chubachi and Y. Kikuchi: "Theoretical Analysis on the

Bragg Diffraction of a Guided Optical Wave by an Acoustic Surface Wave", Trans. IECE Japan, **57-C**, 11, p. 419 (1974).
47) K. Yamanouchi, K. Shibayama and K. Higuchi: "TE-TM Mode Conversion by Acousto-Optic Interaction in Metal Diffused Waveguide", Trans. IECE Japan, **J59-C**, 6, p. 355 (1976).
48) J. Kushibiki, N. Chubachi and K. Shibayama: "Improvement of Diffraction Efficiency in Surface-Acoustic-Optic Device by Means of Multilayered Structure", Appl. Phys. Lett., **29**, 6, p. 333 (1976).
49) N. Goto, Y. Miyazaki and Y. Akao: "Material Dependence of Strain Distributions of Surface Acoustic Waves in Multilayered Thin-Film Acousto-Optic Devices", Jpn. J. Appl. Phys., **24**, 2, p. 148 (1985).
50) A. W. Warner, M. Onoe and G. A. Coquin: "Determination of Elastic and Piezoelectric Constants for Crystals in Class (3m)", J. Acoust. Soc. Am., **42**, 6, p. 1223 (1967).
51) G. Arlt and H. Schweppe: "Paratellurite, a New Piezoelectric Material", Solid-State Commun., **6**, 11, p. 783 (1968).
52) B. A. Auld: Acoustic Fields and Waves in Solids (John Wiley & Sons, New York, 1973).
53) A. A. Oliner: "Waveguides for Acoustic Surface Waves; a Review", Proc. IEEE, **64**, 5, p. 615 (1976).
54) N. Goto, Y. Miyazaki and Y. Akao: "Characteristics of Thin-Film Optical Separators Using Acousto-Optic Effect in Surface Acoustic Waveguides", Jpn. J. Appl. Phys., **24**, Supplement 24-1, p. 127 (1985).
55) N. Goto and Y. Miyazaki: "SAW Propagation Characteristics in Thin-Film Surface Acoustic Waveguides for Acousto-Optic Devices", Trans. IECE Japan, **E69**, 1, p. 47 (1986).
56) N. Goto and Y. Miyazaki: "SAW Propagation Properties in Ta_2O_5 Strip Waveguide for Waveguide-Type Acousto-Optic Devices", Jpn. J. Appl. Phys., **25**, Supplement 25, (1986).
57) L. N. Binh and J. Livingstone: "A Wide-Band Acoustooptic TE-TM Mode Converter Using a Doubly Confined Structure", IEEE J. Quantum Electron., **QE-16**, 9, p. 964 (1980).
58) R. V. Schmidt and L. A. Coldren: "Thin Film Acoustic Surface Waveguides on Anisotropic Media", IEEE Trans. Sonics & Ultrason., **SU-22**, 2, p. 115 (1975).
59) L. A. Coldren: "Acoustic Surface Wave Slot Waveguides on $Bi_{12}GeO_{20}$", IEEE Trans. Sonics & Ultrason., **SU-21**, 2, p. 128 (1974).
60) G. I. Stegeman: "Ⅲ, Optical Probing of Surface Waves and Surface Wave Devices", IEEE. Trans. Sonics & Ultrason., **SU-23**, 1, p. 33 (1976).
61) J. F. Weller and T. G. Giallorenzi: "Optical Detection of Acoustic Surface Waves in Layered Substrates: Theory and Experiment", IEEE Trans. Sonics & Ultrason., **SU-21**, 3, p. 196 (1974).
62) J. B. Green and G. S. Kino: "SAW Convolvers Using Focused Interdigital Transducers", IEEE Trans. Sonics & Ultrason., **SU-30**, 1, p. 43 (1983).
63) Y. Miyazaki and N. Goto: "Integrated Optical Exchange for Multiple Signal Fiber Transmission Systems Using Three Dimensional Surface Acoustic Waveguides", *Proceeding of IEEE Ultrasonic Symposium*, EE-4 (San Francisco, USA, 1985).
64) N. Goto and Y. Miyazaki: "Optical Signal Processors Consisting of Collinear Acousto-Optic Channel Waveguides", *ICASSP'86*, 10A4 (Tokyo, 1986).
65) L. Thylen, A. Djupsjoebacka, M. Janson and W. Doeldissen: "Integrated-Optic Device for High-Speed Databuses", Electron. Lett., **21**, 11, p. 491 (1985).
66) H. F. Taylor: "Technology and Design Considerations for a Very-High-Speed Fiber-Optic Data Bus", IEEE J. Selected Areas in Communications, **SAC-1**, 3, p. 500 (1983).
67) M. Kondo, Y. Ohta, M. Fujiwara and M. Sakaguchi: "Integrated Optical Switch Matrix for Single-Mode Fiber Networks", IEEE J. Quantum Electron., **QE-18**, 10, p. 1759 (1982).
68) L. McCaughan and G. A. Bogert: "4×4 Ti: $LiNbO_3$ Integrated-Optical Crossbar Switch Array", Appl. Phys. Lett., **47**, 4, p. 348 (1985).

69) C. M. Verber: "Integrated-Optical Approaches to Numerical Optical Processing", Proc. IEEE, **72**, 7, p. 942 (1984).
70) C. S. Tsai, D. Y. Zang and P. Le: "Acousto-Optic Bragg Diffraction in a $LiNbO_3$ Channel-Planar composite Waveguide with Application to Optical Computing", Appl. Phys. Lett., **47**, 6, p. 549 (1985).
71) N. Goto and Y. Miyazaki: "Wavelength-Selective Acousto-Optic Switch Consisting of Optical and SAW Channel Waveguides", *OEC'86*, *A9-2* (Tokyo, 1986).